CellPress
OPEN ACCESS

Article

Quantitative increase in T regulatory cells enhances bone remodeling in *osteogenesis imperfecta*

Created with BioRender.com

In-Hong Kang, Uday K. Baliga, Shilpak Chatterjee, ..., Hai Yao, Shikhar Mehrotra, Meenal Mehrotra

mehrotra@musc.edu

Highlights

Activated T cell phenotype and higher secretion of pro-inflammatory cytokines in OI

Quantitative decrease in Tregs observed in OI mice compared with WT mice

Treg transplantation increases Tregs, reduces T cell activation and cytokine secretion

Treg transplantation produces improvements in bone remodeling and mechanical properties

iScience

Article

Quantitative increase in T regulatory cells enhances bone remodeling in *osteogenesis imperfecta*

In-Hong Kang,[1,2] Uday K. Baliga,[1,11] Shilpak Chatterjee,[3,12] Paramita Chakraborty,[3] Seungho Choi,[3] Nathan Buchweitz,[4,5,6] Hong Li,[7] Yongren Wu,[4,5,6] Hai Yao,[4,5,6,8] Shikhar Mehrotra,[3,9] and Meenal Mehrotra[1,3,8,9,10,13,*]

SUMMARY

Osteogenesis imperfecta (OI) is characterized by repeated bone fractures. Recent studies have shown that T lymphocytes and regulatory T cells (Tregs) regulate the functions of osteoclasts and osteoblasts, thus playing a role in bone turnover. We demonstrate an activated effector phenotype and higher secretion of pro-inflammatory cytokines, IFN-γ, and TNF-α in OI peripheral T cells as compared with wild-type (WT). Suppressive Tregs (spleen and thymus) were qualitatively similar, whereas there was a quantitative decrease in OI versus WT. Restoring Treg numbers by systemic transplantation in OI mice resulted in reduced T cell activation and effector cytokine secretion that correlated with significant improvements in tibial trabecular and cortical bone parameters and stiffness of femur, along with increased osteoblast mineralization and decreased osteoclast numbers. Therefore, Tregs can dampen the pro-inflammatory environment and enhance bone remodeling in OI mice. Thus, this study will be helpful in developing future autologous immunotherapy-based treatment modalities for OI.

INTRODUCTION

Osteogenesis imperfecta (OI) is the most common hereditary bone disease. It is characterized by a reduction in bone matrix quantity that leads to repeated fractures with little or no trauma and bone deformity (Shapiro et al., 1995), and is thus often called "brittle bone disease." The therapy goals for patients with OI are to reduce fracture rates, prevent bone deformities, and minimize chronic pain while maximizing bone health (Thomas and DiMeglio, 2016). Although incurable, OI treatment requires a coordinated multidisciplinary team approach and consists of physical therapy, surgical interventions, and medications, especially bisphosphonates. Drug treatment aims to increase overall bone strength, but long-term treatment has detrimental side effects (Uveges et al., 2009). Promising new experimental strategies such as an anti-sclerostin antibody, anti-TGF-β antibody, stem cell therapy, and gene therapy are gaining substantial interest (Thomas and DiMeglio, 2016).

It is known that the immune system can dynamically influence skeletal homeostasis. Recent studies have shown that T lymphocytes could be essential in regulating the homeostasis, survival, and function of osteoclasts and osteoblasts and, thus, play a vital role in bone homeostasis, regeneration, and turnover (Lei et al., 2015; Takayanagi, 2015). Using mice lacking functional lymphocytes, it was shown that T cells play a role in bone regeneration, with the fracture calluses of deficient mice exhibiting poor bone quality (Nam et al., 2012; Toben et al., 2011). Another study showed that delayed fracture healing significantly correlated with enhanced levels of terminally differentiated CD8^{+} effector memory T cells in peripheral blood (Reinke et al., 2013). Massive T cells' infiltration in the fracture callus, especially near newly forming bone, has also been shown (Konnecke et al., 2014). Regulatory T cells (Tregs) are a specialized subpopulation of T cells that suppress the immune response, thereby maintaining immune homeostasis and self-tolerance (Kondelkova et al., 2010). However, whether T cells, specifically Tregs, play a role in OI, a disease with high turnover and high fracture rates, has never been investigated before.

[1]Department of Pathology and Laboratory Medicine, Medical University of South Carolina, Charleston, SC 29425, USA

[2]Department of Microbiology and Immunology, Medical University of South Carolina, Charleston, SC, 29425, USA

[3]Department of Surgery, Medical University of South Carolina, Charleston, SC, 29425, USA

[4]Department of Orthopedics, Medical University of South Carolina, Charleston, SC 29425, USA

[5]Department of Bioengineering, Clemson University, Clemson, SC 29634, USA

[6]Clemson-MUSC Joint Bioengineering Program, South Carolina, USA

[7]Depatment of Public Health Sciences, Medical University of South Carolina, Charleston, SC 29425, USA

[8]Department of Oral Health Sciences, Medical University of South Carolina, Charleston, SC 29425, USA

[9]Hollings Cancer Center, Medical University of South Carolina, Charleston, SC 29425, USA

[10]Center for Oral Health Research, Medical University of South Carolina, Charleston, SC 29425, USA

[11]Present address: Ph.D. student, University of Rochester, Rochester, NY, 14,642, USA

[12]Present address: Senior Scientist, Indian Institute of Chemical Biology, Kolkata, India

[13]Lead contact

*Correspondence: mehrotra@musc.edu

https://doi.org/10.1016/j.isci.2022.104818

Furthermore, bisphosphonates, which are widely used for treating OI, have been shown to cause an elevation in the cytokines IL-10 and TGF-β, which are known to expand and differentiate Tregs in the blood of osteoporotic patients (Talaat et al., 2015). In addition, mice overexpressing Treg signature transcription factor FoxP3 have high bone volume and low osteoclast numbers (Zaiss et al., 2010). Tregs have also been shown to inhibit the differentiation of osteoclasts both in mice (Zaiss et al., 2007) and humans (Kim et al., 2007), and systemic infusion of FoxP3^{+} Tregs markedly improved bone marrow mesenchymal stromal cell-based bone regeneration and calvarial defect repair in C57BL/6 mice (Liu et al., 2011). Thus, we hypothesized that modulation of Treg function has the potential to reinstate bone homeostasis in OI.

This study shows that splenic T cells from OI mice demonstrated an activated phenotype, along with the higher secretion of pro-inflammatory cytokines IFN-γ and TNF-α compared with wild-type (WT) mice. Furthermore, we observed a quantitative decrease in the suppressive natural Tregs (nTregs) from the spleen and thymus in OI mice, even though they were qualitatively similar. On examining the effects of Tregs on OI bone cells, our *in vitro* data demonstrate that conditioned media from WT and OI Tregs not only suppressed osteoclast formation but also caused a remarkable increase in osteoblast mineralization. Furthermore, enhanced improvement in bone parameters was observed when OI mice were transplanted with WT Tregs (allo-transplantation) and OI Tregs (auto-transplantation), which correlated with reduced T cell activation and effector cytokine secretion as well as an increase in the mineralization of osteoblasts and a decrease in osteoclast numbers in transplanted OI mice. Thus, Tregs can dampen the pro-inflammatory environment in OI and contribute to increased osteogenesis and decreased osteoclasts. These studies could pave the way for developing future autologous immunotherapy-based treatment modalities for OI.

RESULTS

Activated phenotype of T cells and enhanced effector cytokine secretion by T cells in OI mice

To investigate the differences in T cell phenotypes in OI mice compared with WT mice, naive T cells from spleens of WT and OI mice were stained with fluorochrome-conjugated anti-CD4, anti-CD8 and anti-CD44 antibodies and analyzed by flow cytometry. The gating strategy is shown in Figure S1. CD44 is a widely expressed adhesion receptor with various cellular functions (Baaten et al., 2010a), including lymphocyte activation, survival, and memory development (Baaten et al., 2010b, 2012). Naive splenic T cells from OI mice exhibited significantly higher expression of CD44 (Figure 1Ai) both in CD4^{+} (upper panel) and CD8^{+} (lower panel) T cells. Moreover, OI mice splenic T cells that were T cell receptor (TCR) activated for three days using anti-CD3 and anti-CD28 antibodies and re-stimulated showed increased levels of intracellular cytokines (to determine cytokine secretion on a per cells basis), IFN-γ (Figure 1Aii) and TNF-α (Figure 1Aiii), both in CD4^{+} T cells (upper panel) and CD8^{+} T cells (lower panel), as compared with T cells from WT mice. On measuring the amount of IFN-γ and TNF-α secreted into the media by CD4 and CD8 cells using ELISA kits, a significant increase in the levels of IFN-γ was observed with both CD4 and CD8 cells from spleens of OI mice as compared with those seen in WT mice (Figure 1Bi, upper panel). Secretion of TNF-α showed a significant increase in only CD8 cells from OI mice compared with WT mice (Figure 1Bi, lower panel). On measuring the IFN-γ and TNF-α levels in the serum of WT and OI mice, there was a trend for a significant increase in IFN-γ levels (Figure 1Bii, upper panel), and a significant increase in TNF-α levels (Figure 1Bii, lower panel) in the serum from OI mice as compared with the serum from WT mice. We also analyzed the mRNA levels of IFN-γ and TNF-α in splenocytes from WT and OI mice. There was a significant increase in the mRNA levels of both IFN-γ (Figure 1Biii, upper panel) and TNF-α (Figure 1Biii, lower panel) in the splenocytes from OI mice as compared with splenocytes from WT mice. These data collectively demonstrate that T cells are in an activated state in the OI mice compared with the WT mice, which results in a pro-inflammatory environment in the OI mice. As activated T cells mediate bone loss (Kong et al., 1999; Weitzmann and Pacifici, 2005), the more activated T cell phenotype in OI may contribute to enhanced disease abnormalities.

Quantity, but not quality, of Tregs is compromised in OI mice

Tregs play an essential role in maintaining peripheral tolerance, and a decrease in their number or suppressive function causes unregulated activation and proliferation of T cells (Sakaguchi et al., 1995). Given the enhanced effector phenotype observed in the OI naive T cells, we determined the number and suppressive activity of the natural regulatory T cells (nTregs). Splenocytes from WT and OI mice were stained with anti-CD4, anti-CD25, and anti-FoxP3 antibodies and analyzed by flow cytometry. The gating strategy is shown in Figure S2. Compared with WT, OI mice had a significant reduction (44.3% ± 10.5%) in the percentage (Figures 1Ci and 1Cii) and the absolute number (Figure 1Ciii) of Tregs. Next, we determined the status
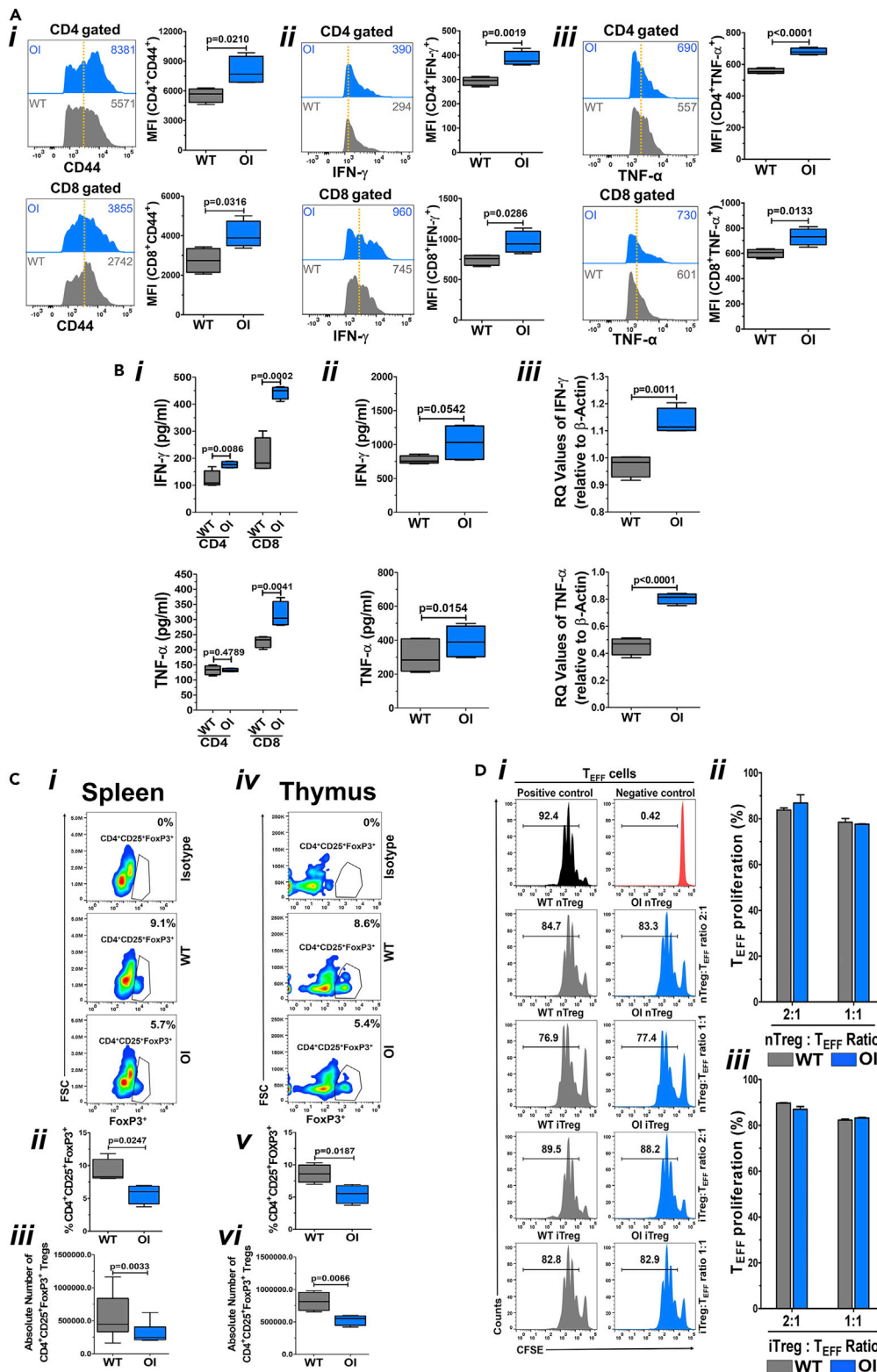
Figure 1. Evaluation of T cells and Tregs in OI mice

(A) Activated phenotype of T cells and enhanced effector cytokine secretion by T cells in OI mice. Spleen-derived naive T cells from WT and OI mice were stained using fluorochrome-conjugated CD44 antibody, acquired by FACS, and

Figure 1. *Continued*

analyzed by FlowJo software (Ai). Data from one of three experiments with a similar result are shown in the left panel. The dotted vertical line indicates the mean position of the peak in WT T cells to compare relative expression between samples visually. Mean MFI values (from all experiments) for CD44 in OI T cells are significantly greater than those seen in WT T cells (right panel). This can be seen in both CD4 (upper panel) and CD8 (lower panel) cells. Splenic T cells from WT and OI mice were activated for three days using anti-CD3 and anti-CD28 antibodies before being re-stimulated with similar stimuli in the presence of Golgi-Plug. Intracellular staining was done with fluorochrome-conjugated antibodies, and data were acquired using FACS. IFN-γ is shown in (Aii), whereas TNF-α is shown in (Aiii). Data from one of three experiments with a similar result are shown in *the left panels*. The numerical values within each display are MFI, and the dotted vertical line indicates the mean position of the peak in WT T cells. Mean MFI values (from all experiments) show that there is a significantly greater expression of both IFN-γ and TNF-α in OI T cells as compared with WT T cells (*right panels*) in both CD4 (upper panel) and CD8 (lower panel) cells. Data are presented as Mean ± SD.

(B) Secretion of pro-inflammatory cytokines. Media from splenocyte derived CD4 and CD8 cell cultures was collected and IFN-γ and TNF-α levels were analyzed using ELISA assay (Bi). There is a significant increase in IFN-γ levels in both CD4 and CD8 OI T cell cultures as compared with WT T cell cultures (upper panel). TNF-α levels were significantly increased in only CD8 OI T cells compared with WT T cells (lower panel). IFN-γ and TNF-α levels were also analyzed in serum of WT and OI mice (n = 4) using ELISA assay (Bii). A trend for significant increase is seen in IFN-γ levels (upper panel), whereas a significant increase is seen in TNF-α levels (lower panel) in OI mice serum compared with WT mice serum. mRNA expression of IFN-γ and TNF-α was analyzed in splenocytes using real-time PCR (Biii). A significant increase is seen in both IFN-γ (upper panel) and TNF-α (lower panel) expression in OI mice splenocytes compared with WT mice splenocytes. Data are presented as Mean ± SD.

(C) Reduced number of Tregs in OI mice. Cells from the spleen (Ci, ii, and iii) and thymus (Civ, v, and vi) were stained using fluorochrome-conjugated CD4, CD25, and FoxP3 antibodies to compare the percent of Tregs between WT and OI mice. Flow cytometric plots of the representative data (Ci and iv), and the graph of the cumulative data of percentages of Treg (Cii and v) as well as the absolute number of Tregs (Ciii and vi), demonstrates that there is a significant decrease in the number of Tregs both in the spleen (Ci, ii, and iii) and the thymus (Civ, v, and vi) of OI mice compared with WT mice. Data are presented as Mean ± SD.

(D) Similar Treg functionality in WT and OI mice. nTregs and iTregs from spleens of WT and OI mice were co-cultured with spleen T cell (T_{EFF}; responder cells) from WT mice (labeled with CFSE), in a ratio of 1:1 and 1:2, and stimulated with anti-CD3 and anti-CD28 antibodies for three days. For controls, CFSE labeled WT T cells were cultured in the absence of anti-CD3 and anti-CD28 antibodies. After three days, cells were stained for CD4 and analyzed for CFSE dilution by flow cytometry. nTregs, as well as iTregs from both WT and OI mice, suppressed T cells to the same extent, at both the ratios, as can be seen in flow cytometry plots from a representative experiment (Di) and the graphs of the cumulative data for nTregs (Dii) and iTregs (Diii). Data are presented as Mean ± SD.

of thymic Tregs that contribute to central tolerance (Caramalho et al., 2015; Lee and Lee, 2018). A significant decrease (36.9% ± 11.8%) in the percentage (Figure 1Civ and 1Cv) and the absolute number (Figure 1Cvi) of CD4$^+$CD25$^+$FoxP3$^+$ cells in thymocytes from OI mice compared with WT mice was observed. This indicates that OI mice have an overall reduction in Tregs, leading to increased T cell activation and enhanced effector cytokine secretion.

To examine the quality of Tregs, we obtained nTregs (CD4$^+$CD25$^+$) and iTregs (CD4$^+$CD25$^-$ cells cultured with anti-CD3, anti-CD28, IL-2, TGF-β, and retinoic acid for three days) (Chatterjee et al., 2014) from spleens of WT and OI mice, as detailed in the Methods. After that, the suppressive function of Tregs was determined by using CFSE labeled CD4$^+$CD25$^-$ splenic T cells (T_{EFF}; responder cells) from WT mice in co-culture with nTregs and iTregs (in a ratio of 1:1 and 1:2) that were stimulated with anti-CD3 and anti-CD28 antibodies (5 ug/ml each) for three days. Analysis for CFSE dilution after three days showed that nTregs and iTregs from both WT and OI mice suppressed T cell proliferation to the same extent, at both the ratios, as evident in the flow cytometry graphs (Figure 1Di), and the cumulative data from n = 3 mice for nTregs (Figure 1Dii) and iTregs (Figure 1Diii). These data indicate that Tregs in OI mice are qualitatively similar compared with WT mice. Thus, the increased activated T cell phenotype in OI mice is not attributed to dysfunctional Tregs but their reduced numbers.

Treg-conditioned media decreases osteoclast number and increases osteoblast mineralization

To determine how reduced Treg numbers impacted bone formation in OI mice, we first examined its role on osteoclasts and osteoblasts by setting up *in vitro* cultures in the presence of Treg-conditioned media. Osteoclasts and osteoblast from OI mice were grown in their respective media (α-MEM/10%FBS/PS/RANKL/M-CSF for osteoclasts; α-MEM/10%FBS/PS/L-glut/AA/BGP for osteoblasts) supplemented with 50% control media or conditioned media from either WT Tregs or OI Tregs. The osteoblast and osteoclast
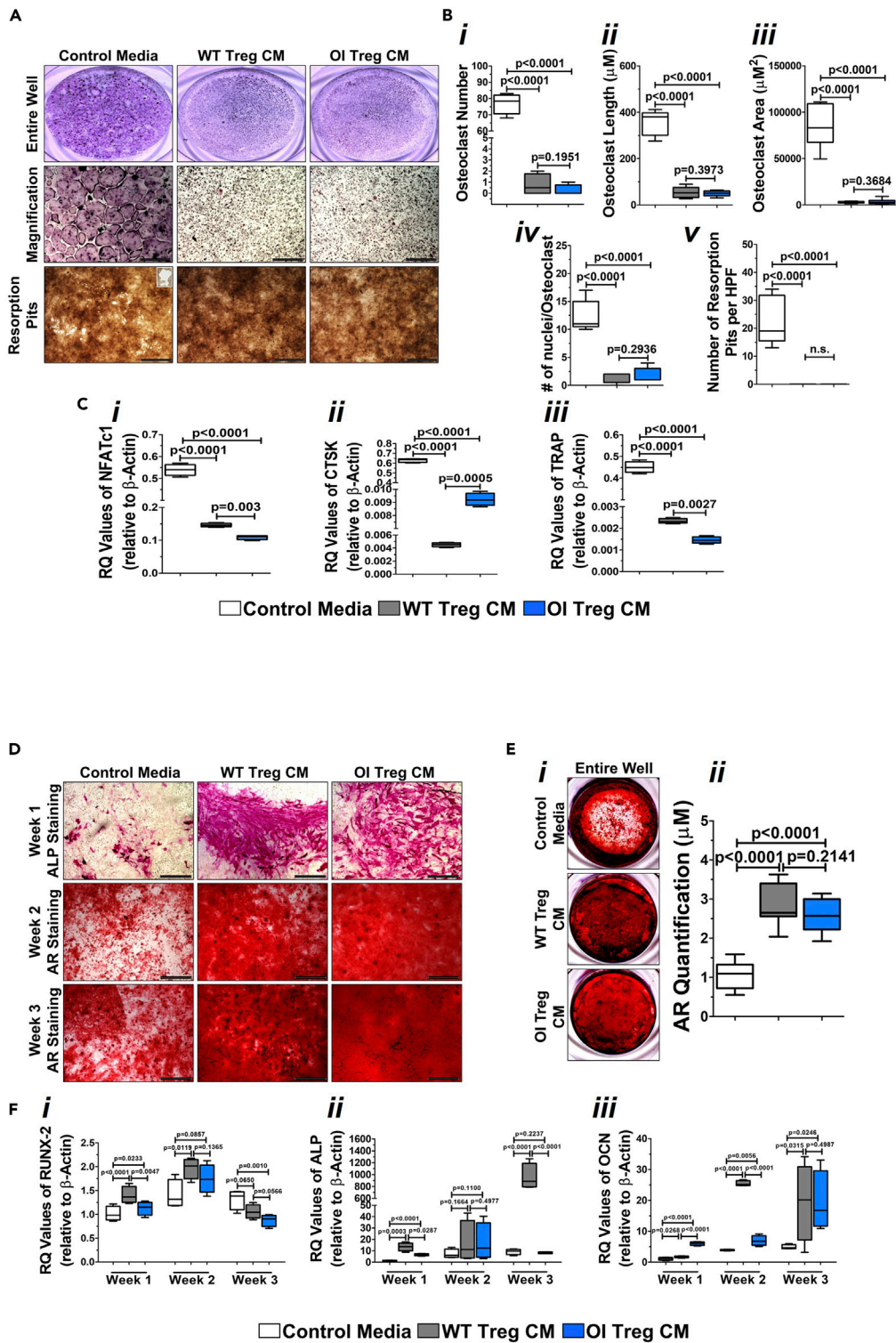
Figure 2. Effect of Treg-conditioned media on osteoclasts and osteoblasts from OI mice

(A and B) Treg-conditioned media decreases the osteoclast number and activity. Non-adherent bone marrow cells from OI mice were grown in the presence of control osteoclast media, or osteoclast media supplemented with 50% WT and OI Treg-conditioned media and TRAP staining conducted. A significant decrease in the number of osteoclasts was observed with either WT- or OI Treg-conditioned media than control media. This is evident in the representative images (A, top and

Figure 2. *Continued*

middle panels) and the cumulative graph (Bi). The osteoclast length (Bii), osteoclast area (Biii), and the number of nuclei per osteoclast (Biv) was significantly lower in cultures treated with WT- and OI Treg-conditioned media compared with control media. A significant decrease was seen in the number of resorption pits in the presence of WT- and OI Treg-conditioned media as evident in the representative images (A, bottom panel) and cumulative graph (Bv). Data are presented as Mean $\pm$ SD. Bar = 100μM.

(C) Treg-conditioned media decreases the expression of osteoclast-specific genes. RNA was extracted from osteoclasts grown in control media and WT- and Treg-conditioned media and real-time PCR was conducted. A significant decrease was seen in mRNA expression of NFATc1 (Ci), CTSK (Cii), and TRAP (Ciii) in the presence of WT- and OI Treg-conditioned media when compared with control media. Data are presented as Mean $\pm$ SD.

(D) Treg-conditioned media increases alkaline phosphatase and alizarin red staining in osteoblasts. OI long bone cells were cultured in osteogenic control media and osteogenic media supplemented with 50% conditioned media from WT and OI Tregs. Alkaline phosphatase staining was conducted in week 1, whereas cultures in weeks 2 and 3 were stained with alizarin red. There was a significant increase in alkaline phosphatase staining in week 1 with WT- and OI Treg-conditioned media compared with control media (D, top panel). Furthermore, alizarin red staining was increased in weeks 2 (D, middle panel) and 3 (D, bottom panel) in the presence of WT- and OI Treg-conditioned media as compared with control media. Bar = 100μM.

(E) Treg-conditioned media increases calcium deposition by osteoblasts. Alizarin red staining of wells with osteoblast cultures indicated a significant increase in the calcium deposition in the presence of conditioned media from both WT and OI Tregs when compared with control media, which is evident in both the representative images of the wells (Ei) as well as in the cumulative graph (Eii). Data are presented as Mean $\pm$ SD.

(F) Treg-conditioned media increases the expression of osteoblast-specific genes. RNA was extracted from osteoblasts grown in control media and WT- and Treg-conditioned media at weeks 1, 2, and 3 and real-time PCR was conducted. A significant increase or a trend for significant increase was seen in the expression of Runx-2 in weeks 1 and 2, whereas the expression decreases in week 3 in the presence of WT and OI Treg-conditioned media compared with control media (Fi). Alkaline phosphatase was significantly increased at weeks 1 and 3 more with WT Treg-conditioned media than with OI Treg-conditioned media (Fii). Osteocalcin expression was significantly increased in the presence of WT- and OI Treg-conditioned media at weeks 1, 2, and 3, compared with control media (Fiii). Data are presented as Mean $\pm$ SD.

media were made as a 2X concentrated mix and then mixed with the serum-free conditioned media. TRAP staining of osteoclast cultures demonstrated a significant decrease in the number of osteoclasts when treated with conditioned media from either WT or OI Tregs, as evident in representative images of the wells (Figure 2A, top panel, middle panel) as well in the cumulative graph of *n* = 5 experiments (Figure 2Bi). There was a significant reduction in the length and the area of the osteoclasts in the presence of WT- and OI Treg-conditioned media (Figures 2Bii and 2Biii). The number of nuclei per osteoclasts also significantly decreased with WT- and OI Treg-conditioned media (Figure 2Biv). There was also a significant reduction in the activity of osteoclasts in the presence of WT- and Treg-conditioned media as measured by the formation of resorption pits seen in the images (Figure 2A, bottom panel) and the cumulative graph (Figure 2Bv). There were no differences in any of the WT- and OI Treg-conditioned media parameters. A significant reduction was also observed in the expression of osteoclast-specific genes, NFATc1 (Figure 2Ci), CTSK (Figure 2Cii), and TRAP (Figure 2Ciii) in the presence of both WT- and OI Treg-conditioned media. The expression of NFATc1 and TRAP was significantly lower in the presence of OI Treg-conditioned media as compared with WT Treg-conditioned media (Figure 2C1, 2Ciii), whereas the same was not true for CTSK (Figure 2Cii). Osteoblastic cultures were stained for alkaline phosphatase in week 1 of culture and alizarin red in weeks 2 and 3. As seen in the images, there was a significant increase in alkaline phosphatase as well as alizarin red staining at all time points in the presence of WT- and OI Treg-conditioned media (Figure 2D). Alizarin red staining of the entire wells indicated a significant increase in the calcium deposition by the osteoblasts in the presence of conditioned media from both WT and OI Tregs when compared with control media, which is evident in both the representative images of the wells (Figure 2Ei) as well in the cumulative graph of *n* = 5 experiments (Figure 2Eii). There was no difference between the calcium deposition seen with WT- and OI Treg-conditioned media. There was a significant increase or a trend for a significant increase in the expression of Runx-2 in weeks 1 and 2 of culture, whereas the expression decreased by week 3 in the presence of WT- and OI Treg-conditioned media, indicating a more differentiated phenotype of the osteoblasts (Figure 2Fi). Alkaline phosphatase was significantly increased at weeks 1 and 3, more so in the presence of WT Treg- than OI Treg-conditioned media (Figure 2Fii). No differences were observed in week 2. Osteocalcin expression levels were significantly increased in the presence of both WT- and OI Treg-conditioned media at weeks 1, 2, and 3 of cultures (Figure 2Fiii). These data indicate that conditioned media from Tregs decrease the osteoclast number and activity as well as increase the osteoblast mineralization in OI
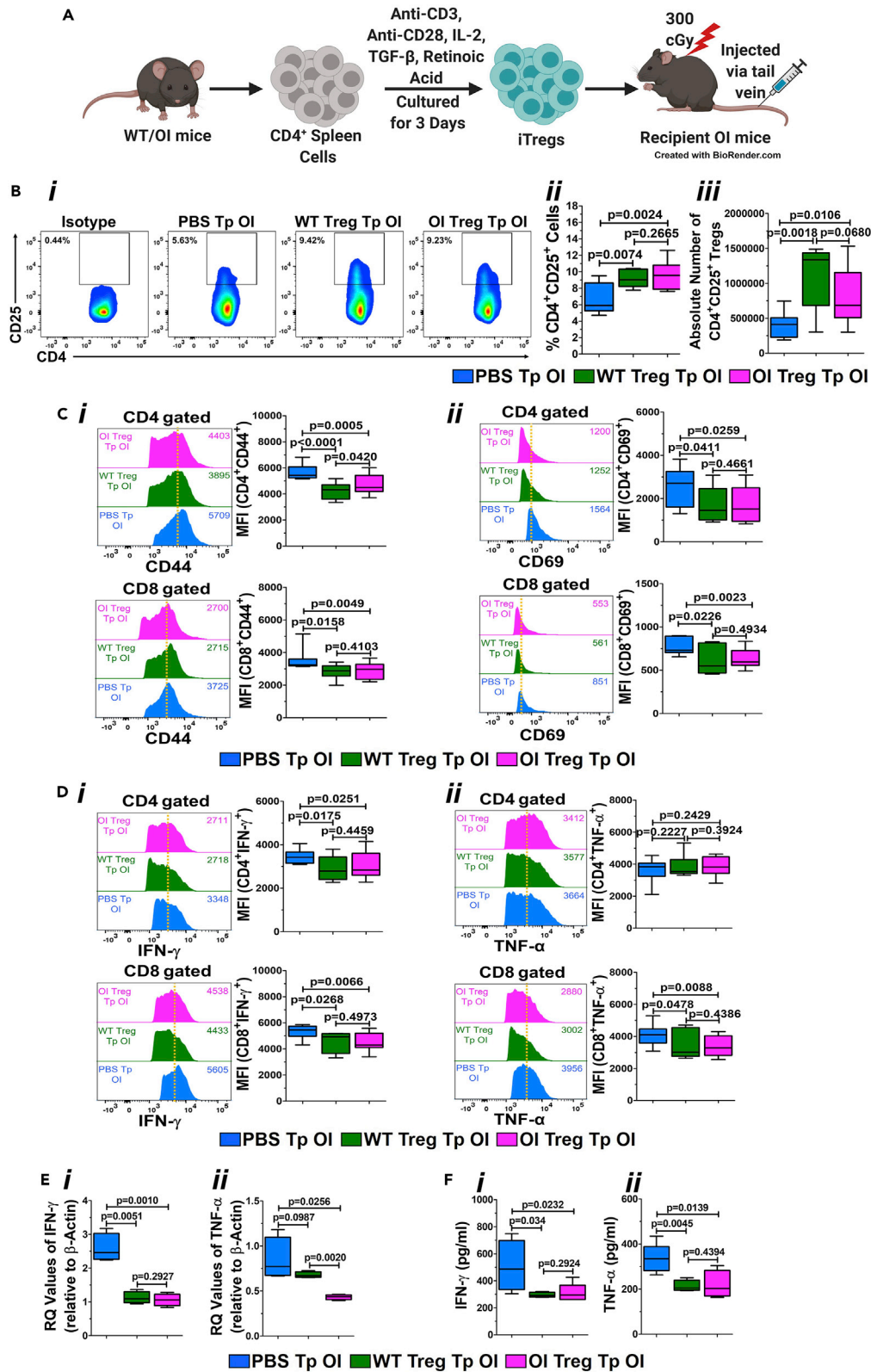
Figure 3. Treg transplantation in OI: effect on T cells and Tregs

(A) *In vivo* iTreg transplantation. One million iTregs, generated from both WT and OI mice were transplanted into recipient OI mice, irradiated at 300 cGy, intravenously via the tail vein. OI mice injected with PBS served as controls. This illustration was created using BioRender.

(B) Quantitative increase in the number of Tregs in OI mice after Treg transplantation. Splenocytes from PBS-, WT Treg-, and OI Treg-transplanted OI mice were stained with anti-CD4 and anti-CD25 antibodies and analyzed by flow cytometry. Flow cytometric plots of the representative data (Bi), and the graph of cumulative percentages (Bii) and absolute numbers of Tregs (Biii), demonstrate a significant increase in Tregs in OI mice after both WT and OI Treg transplantations. Data are presented as Mean $\pm$ SD.

(C) Reduced T cell Activation in OI Mice after Treg Transplantation. Spleen-derived naive T cells were obtained from PBS-, WT Treg-, and OI Treg-transplanted OI mice, stained using fluorochrome-conjugated CD44 (Ci) and CD69 (Cii) antibodies, acquired by FACS and analyzed by FlowJo software. Representative flow cytometric plots from each group are sown in the left panel. The dotted vertical line indicates the mean position of the peak in PBS-transplanted OI mice T cells to compare relative expression between samples visually. Mean MFI values from individual analyses of $n = 7$–9 mice per group is shown in the right panel. The upper panel shows CD4 cells, and the lower panel shows CD8 cells. There was a significant decrease in the expression of CD44 (Ci) and CD69 (Cii) in both CD4 and CD8 cells after WT and OI Treg transplantation compared with PBS-transplanted control. Data are presented as Mean $\pm$ SD.

(D) Reduced effector cytokines in T Cells in OI mice after Treg transplantation. Splenic T cells from PBS-, WT-, and OI Treg-transplanted OI mice were activated for three days using anti-CD3 and anti-CD28 antibodies before being re-stimulated with similar stimuli in the presence of Golgi-Plug. Intracellular staining was done with fluorochrome-conjugated antibodies, and data were acquired using FACS and analyzed using FlowJo software. IFN-γ is shown in (Di), whereas TNF-α is shown in (Dii). Representative flow cytometric plots from each group are sown in the left panel. The numerical values within each display are MFI, and the dotted vertical line indicates the mean position of the peak in PBS-transplanted control T cells. Mean MFI values from individual analyses of $n = 7$–9 mice per group is shown in the right panel. The upper panel shows CD4 cells, and the lower panel shows CD8 cells. IFN-γ levels in OI mice were significantly reduced after transplantation of WT and OI Tregs compared with PBS-transplanted OI mice in both CD4 and CD8 T cells (Di). There was no change in TNF-α expression levels in CD4 T cells, but a significant decrease was seen in CD8 T cells in OI mice after WT and OI Treg transplantation compared with PBS control (Dii). Data are presented as Mean $\pm$ SD.

(E) Reduced expression of pro-inflammatory cytokines. mRNA expression of IFN-γ and TNF-α after transplantation was analyzed in splenocytes using real-time PCR. A significant decrease is seen in both IFN-γ (Ei) and TNF-α (Eii) expression in splenocytes from OI mice transplanted with WT and OI Tregs as compared with splenocytes from PBS-transplanted OI mice. Data are presented as Mean $\pm$ SD. (F) Reduced levels of pro-inflammatory cytokines in the serum. IFN-γ and TNF-α levels were analyzed in serum of transplanted OI using an ELISA assay. A significant decrease is seen in both IFN-γ (Fi) and TNF-α (Fii) levels in OI mice transplanted with WT and OI Tregs compared with OI mice transplanted with PBS. Data are presented as Mean $\pm$ SD.

mice cells and, most importantly, illustrate that OI Treg-conditioned media had similar effects to the WT Treg-conditioned media.

Treg transplantation reduces activated T cell phenotype in OI mice

As we observed a reduction in the number of Tregs in OI mice and an effect of Treg-conditioned media on osteoclasts and osteoblasts from OI mice *in vitro*, we wanted to examine the impact of increasing the Tregs numbers in OI mice *in vivo*. Thus, OI mice were transplanted with Tregs. iTregs were generated from both WT and OI mice, and one million Tregs were then transplanted into recipient OI mice, irradiated at 300 cGy, intravenously via the tail vein (Figure 3A). OI mice injected with PBS served as controls. Transplanted OI mice demonstrated an increase in the percentage of CD4$^+$CD25$^+$ Tregs after WT and OI Treg transplantation. PBS-transplanted OI mice showed around 6.3% $\pm$ 1.7% Tregs in circulation, whereas the Tregs in WT- and OI Treg-transplanted OI mice were 9.5% $\pm$ 0.9% and 9.6% $\pm$ 1.4%, respectively (Figure 3Bi). Similar data were observed in repeat transplantation experiments, as shown in the cumulative graph from $n = 7$ to 9 mice (Figure 3Bii). In addition to the percentage of Tregs, the absolute number of Tregs was also significantly increased after transplantation with WT and OI Tregs (Figure 3Biii). There was no difference between Treg numbers after WT Treg transplantation and OI Treg transplantation.

To confirm if there was a change in the T cell activation phenotype of the recipient OI mice after Treg transplantation, analysis of splenic T cells for activation markers, CD44 (Baaten et al., 2010a, 2010b, 2012) and CD69 was done by flow cytometry. CD69 is a membrane-bound, type II C-lectin receptor, an early marker of lymphocyte activation owing to its rapid appearance on the plasma membrane's surface after stimulation (Cibrian and Sanchez-Madrid, 2017; Ziegler et al., 1994). The gating strategy is shown in Figure S1. A significant decrease in the expression of CD44 (Figure 3Ci) and CD69 (Figure 3Cii) in both CD4$^+$ T cells
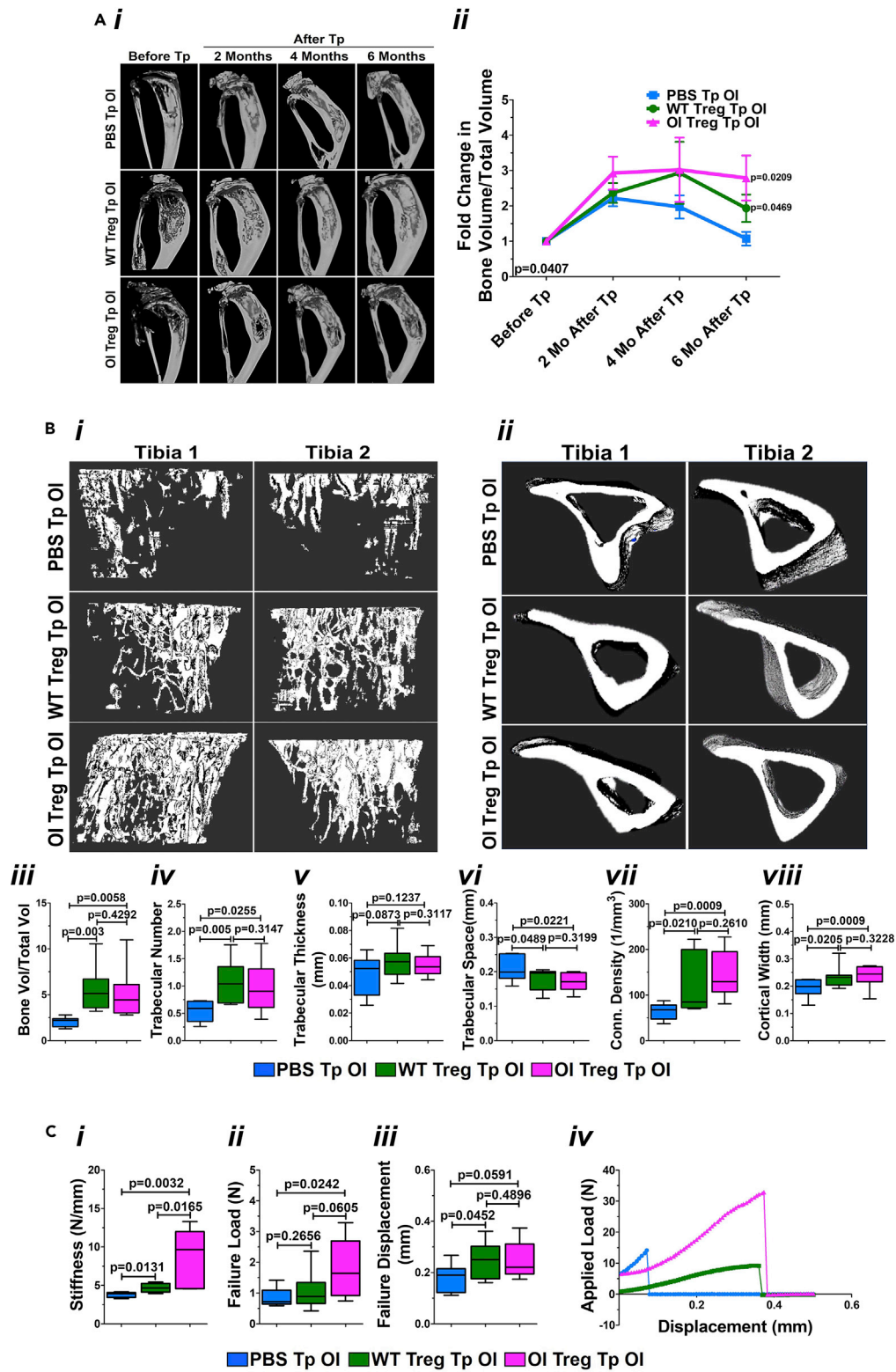
Figure 4. Treg transplantation in OI: effect on bone parameters

(A) Improved bone architecture and bone volume on longitudinal micro-CT in OI mice after Treg transplantation. Longitudinal micro-CT was performed at two, four, and six months post transplantation and compared with respective baseline pre-transplant control. Representative images of the tibia from a PBS-transplanted, WT Treg-transplanted, and

Figure 4. *Continued*

OI Treg transplanted OI mice show progressive improvements in bone architecture after Treg transplantation (Ai). On plotting a fold change in the bone volume/Total volume, a significant increase is seen in OI mice after WT and OI Treg transplantation (Repeated Measures ANOVA; *p*-value = 0.0407) (Aii), specifically at six months after transplantation. Data are presented as Mean ± SD.

(B) Increase trabecular bone and morphometry on *ex vivo* micro-CT in OI mice after Treg transplantation. *ex vivo* micro-CT of the tibia from PBS-, WT Treg-, and OI Treg-transplanted OI mice was conducted six months after transplantation. Representative images of proximal tibiae from two mice showed increased trabecular bone in WT- and OI Treg-transplanted OI mice compared with PBS-transplanted OI mice (Bi). Images also show improvements in the tibial cortical bone after transplantation (Bii). A significant increase in BV/TV (Biii) and trabecular number (Biv) with no change in trabecular thickness (Bv) and a significant decrease in trabecular spacing (Bvi) can be seen after both WT and OI Treg transplantations. Connectivity density was also significantly increased after WT and OI Treg transplantation (Bvii). A significant increase in cortical width can be seen after both WT and OI Treg transplantations as compared with PBS transplantation (Bviii). Data are presented as Mean ± SD.

(C) Improved mechanical properties in OI mice after Treg transplantation. Mechanical properties were examined by analyzing femur from PBS-, WT Treg-, and OI Treg-transplanted OI mice by three-point bending, six months post-transplantation. Stiffness showed a significant increase after both WT and OI Treg transplantation (Ci). Failure load was the same after WT Treg transplantation but significantly increased after OI Treg transplantation, compared with PBS controls (Cii). Failure displacement was also significantly increased after WT and OI Treg transplantation as compared with PBS transplantation (Ciii). The deflection curve (applied load versus displacement) for a representative mouse per group is shown in Civ. PBS-transplanted OI femur shows very little displacement with applied load before breaking. WT Treg-transplanted OI femur shows increased displacement before breaking but with a smaller applied load. OI Treg-transplanted OI femur demonstrates an increased applied load as well as a displacement before breaking. Data are presented as Mean ± SD.

(upper panel) and CD8$^+$ T cells (lower panel) was observed after transplantation of OI mice with WT as well as OI Tregs compared with OI mice transplanted with PBS. A concomitant decrease was observed in effector cytokine IFN-γ secretion in both CD4$^+$ and CD8$^+$ T cells in OI mice after transplantation of WT and OI Tregs (Figure 3Di, upper and lower panel). No changes in the TNF-α expression levels in CD4$^+$ T cells were seen after WT and OI Treg transplantation (Figure 3Dii, upper panel), whereas a significant decrease in CD8$^+$ T cells (Figure 3Dii, lower panel) was observed. Furthermore, there was a significant decrease in the mRNA expression levels of IFN-γ (Figure 3Ei) and TNF-α (Figure 3Eii) in the splenocytes after both WT and OI Treg transplantation. Furthermore, there was a significant decrease in the expression of TNF-α after OI Treg transplantation when compared with WT Treg transplantation (Figure 3Eii). Lastly, the levels of IFN-γ (Figure 3Fi) and TNF-α (Figure 3Fii), measured by ELISA, were significantly reduced in the serum of OI mice after both WT and OI Treg transplantation as compared with the PBS-transplanted OI mice. No differences were observed between the WT- and OI Treg-transplanted mice. These data indicate a reduction in the pro-inflammatory environment in the OI mice after Treg transplantation.

Treg transplantation in OI mice improves the bone architecture, morphometry, and mechanical strength

We analyzed bone parameter changes as the pro-inflammatory environment decreased in OI mice after Treg transplantation. Longitudinal micro-CT was performed at two, four, and six months post-transplantation compared with respective baseline pre-transplant control. Representative images of the tibia from a PBS-, WT Treg-, and OI Treg-transplanted OI mice show progressive improvements in bone architecture after WT and OI Treg transplantation at all time points in contrast to the PBS-transplanted OI (Figure 4Ai). On morphometric analysis (*n* = 7–9 mice/group), there was a significant increase in the bone volume/total volume (BV/TV) after WT and OI Treg transplantation (significance analyzed by Repeated Measures ANOVA; *p*-value = 0.0407; presented as fold change in the BV/TV at two, four, and six months after transplant compared with before transplant control) (Figure 4Aii). In addition, an increase in BV/TV in all three groups at two months after transplantation compared with baseline pre-transplantation levels was observed. However, the BV/TV decreases in PBS-transplanted OI at four and six months after transplantation, but it remains elevated in WT- and OI Treg-transplanted OI at four and six months after transplantation. At six months after transplantation, though there was a significant increase in BV/TV in WT- and OI Treg-transplanted OI mice compared with PBS-transplanted OI mice, BV/TV showed a decrease in WT Treg-transplanted OI compared with that seen at four months, whereas it remained elevated in OI Treg-transplanted OI mice.
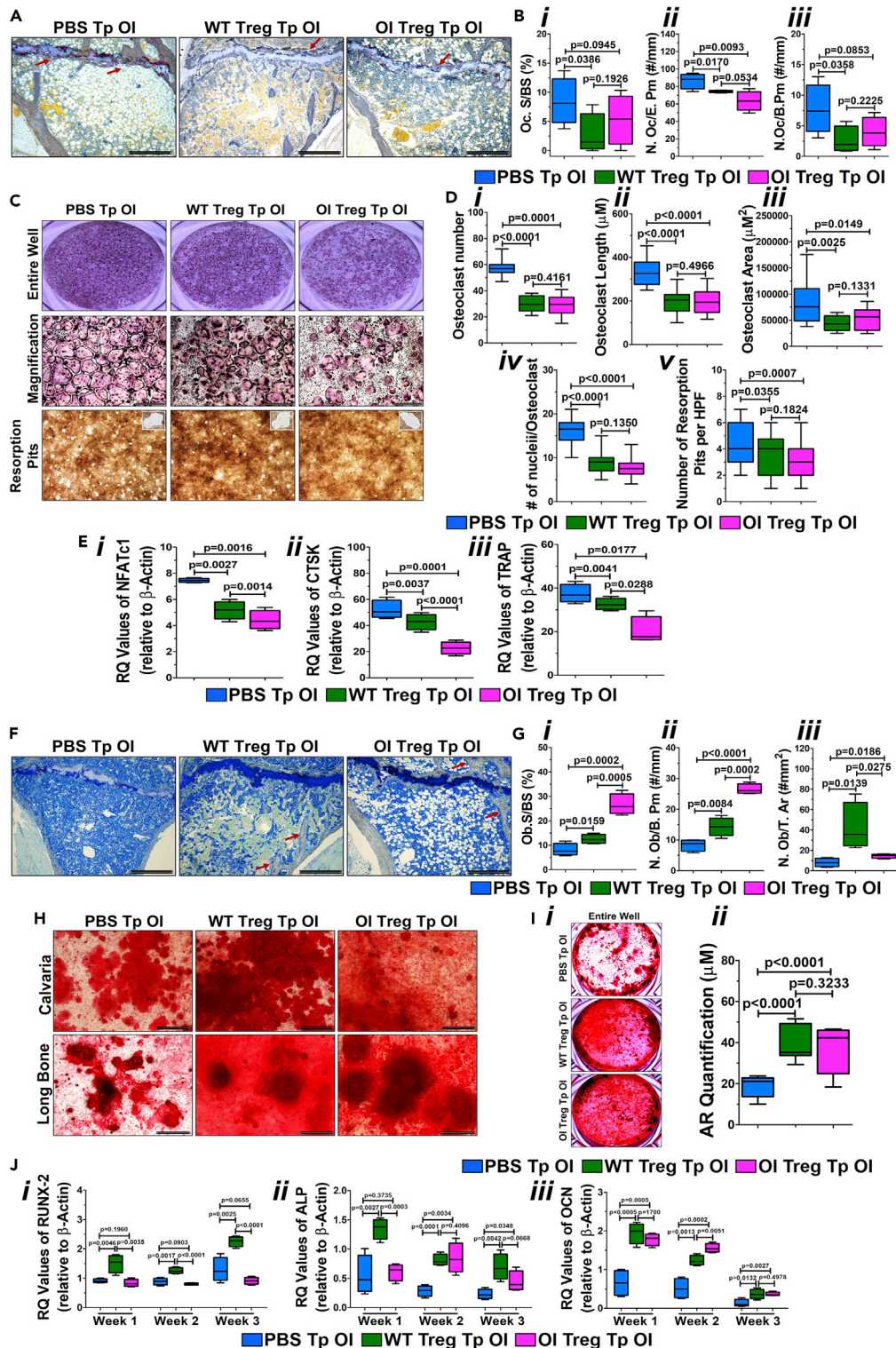
Figure 5. Treg transplantation in OI: effect on osteoclasts and osteoblasts

(A) Decrease in TRAP staining after transplant. MMA embedded tibial sections were stained with TRAP. A decrease in staining for osteoclasts can be seen in the sections (A; brown stain; red arrows). Bar = 100 μM.

(B) Decrease in osteoclastic parameters on histomorphometry. Percentage of osteoclast surface per bone surface (Oc.S/BS) (Bi) and the number of osteoclasts per erosion perimeter (N.Oc/E.Pm) (Bii) were significantly decreased in WT- and

Figure 5. *Continued*

OI Treg-transplanted OI compared with PBS-transplanted OI, whereas the number of osteoclasts per bone perimeter (N. Oc/B.Pm) was significantly decreased in WT Treg-transplanted OI mice but showed a trend for decrease in OI Treg-transplanted OI mice (Biii). Data are presented as Mean ± SD.

(C and D) Decrease in osteoclast numbers and activity. Bone marrow from tibia/femur from individual transplanted mice was used to set up osteoclast cultures. TRAP staining of osteoclast cultures demonstrated a significant decrease in the number of osteoclasts in cultures from WT- and OI Treg-transplanted OI mice as compared with PBS-transplanted OI mice as seen in the representative images of the wells (C, top panel, middle panel) and in the cumulative graph (Di). A significant reduction in the length (Dii), area (Diii), and number of nuclei per osteoclast (Div) was seen in cultures from WT- and OI Treg-transplanted OI mice when compared with cultures from PBS-transplanted mice. The number of resorption pits were significantly lower in WT- and OI Treg-transplanted OI mice as compared with PBS-transplanted OI mice as seen in the representative images (C, bottom panel) and the cumulative graph (Dv). Data are presented as Mean ± SD. Bar = 100μM.

(E) Decrease in the expression of osteoclast-specific genes. The mRNA expression of osteoclast-specific genes was analyzed by real-time PCR. NFATc1 (Ei), CTSK (Eii), and TRAP (Eiii) were significantly reduced in both WT- and OI Treg-transplanted OI mice compared with PBS-transplanted OI mice with expression being significantly lower in OI Treg-transplanted OI mice osteoclasts as compared with WT Treg-transplanted OI mice osteoclasts. Data are presented as Mean ± SD.

(F) Increase in trabeculae. MMA-embedded tibial sections were stained with toluidine blue. There was an increase in the trabeculae after WT and OI Treg transplantation as compared with PBS transplantation (F; red arrows). Bar = 100μM.

(G) Increase in the osteoblast number. Histomorphometric analysis was conducted on the toluidine blue stained tibial sections. A significant increase in the percentage of osteoblasts surface/bone surface (Ob.S/BS) (GI), the number of osteoblasts per bone perimeter (N.Ob/B.Pm) (Gii), and the number of osteoblasts per total area (N.Ob/T.Ar) (Giii) was seen after WT and OI Treg transplantations as compared with PBS transplantation. Data are presented as Mean ± SD.

(H and I) Increase in calcium deposition. Calvarial and long bone cells from individual transplanted mice were grown under osteogenic conditions for three weeks and stained with alizarin red. Increased calcium deposition is visible in representative images of both long bone and calvarial cultures from WT- and OI Treg-transplanted OI mice as compared with PBS-transplanted OI mice, evident from increased alizarin red staining (H). The increase in calcium deposition is significant as seen in the representative images of alizarin red staining of the entire well (Ii) and in the cumulative graph of alizarin red quantification (Iii). Data are presented as Mean ± SD. Bar = 100μM.

(J) Increase in osteoblast-specific genes. mRNA was extracted from osteoblast cultures and expression of osteoblast specific genes was measured by real-time PCR. A significantly higher expression of Runx-2 (Ji), alkaline phosphatase (Jii), and osteocalcin (Jiii) mRNA expression levels is observed in osteoblasts from WT- and OI-transplanted OI mice as compared with PBS-transplanted OI mice as almost all the time points during osteoblast differentiation. Data are presented as Mean ± SD.

To comprehensively examine the bone architecture, *ex vivo* micro-CT was performed on the tibia obtained from PBS-, WT Treg-, and OI Treg-transplanted OI mice six months after transplantation. Images of proximal tibiae from two different mice (to show that similar results were obtained in the mice after the transplantation) demonstrated increased trabecular bone in WT- and OI Treg-transplanted OI mice compared with PBS-transplanted OI mice (Figure 4Bi). Improvements in the cortical bone can also be appreciated after WT Treg and OI Treg transplantations compared with PBS transplantation (Figure 4Bii). Bone morphometric analysis (*n* = 7–9 mice per group) showed a significant increase in BV/TV (Figure 4Biii) and trabecular number (Figure 4Biv) with no change in trabecular thickness (Figure 4Bv) after both WT and OI Treg transplantations. Trabecular spacing was significantly decreased in WT- and OI Treg-transplanted OI mice compared with PBS-transplanted OI mice (Figure 4Bvi). Connectivity density was also significantly increased after WT and OI Treg transplantation (Figure 4Bvii). Cortical width also showed a significant increase after both WT and OI Treg transplantations compared with PBS transplantation (Figure 4Bviii). Mechanical properties were examined by analyzing femurs from PBS-, WT Treg-, and OI-Treg transplanted OI mice (*n* = 7–9 mice per group) by three-point bending, six months post-transplantation (Figure 4C). A significant increase was observed in stiffness after WT and OI Treg transplantation (Figure 4Ci). There was no change in the failure load after WT Treg transplantation, but a significant increase was observed after OI Treg transplantation (Figure 4Cii). Failure displacement showed a significant increase after WT Treg transplantation and a trend for increase after OI Treg transplantation compared with PBS transplantation (Figure 4Ciii). The deflection curve (plotting applied load versus displacement) for an individual mouse per group is shown in Figure 4Civ. PBS-transplanted OI femur shows minimal displacement with the applied load before breaking. WT Treg-transplanted OI femur shows increased displacement before breaking, but the applied load is more diminutive. On the other hand, OI Treg-transplanted OI femur demonstrates an increased applied load as well as displacement before breaking. This indicates an increase in the

strength of the femur after transplantation. These data suggest that WT and OI Treg transplantation in OI mice improves overall bone architecture, morphometry, and mechanical properties.

Reduced osteoclast number and increased osteoblast differentiation after Treg transplantation

To examine if Treg transplantation can affect osteoclasts and osteoblasts *in vivo*, we performed histomorphometry. Sections of the tibia demonstrated a decreased TRAP staining for osteoclasts (Figure 5A; seen as a brown stain; red arrows). Morphometric analysis (n = 7–9 mice per group) shows a significant decrease in the percentage of osteoclast surface/bone surface (Oc.S/BS) in the WT- and OI Treg-transplanted OI compared with PBS-transplanted OI (Figure 5Bi). The number of osteoclasts per erosion perimeter (N.Oc/E.Pm) was also significantly decreased in WT- and OI Treg-transplanted OI mice (Figure 5Bii). The number of osteoclasts per bone perimeter (N. Oc/B.Pm) was significantly decreased in WT Treg-transplanted OI mice but showed a trend for a decrease in OI Treg-transplanted OI mice (Figure 5Biii). Moreover, we collected bone marrow from the tibia/femur from transplanted OI mice and set up osteoclast cultures as detailed in the Methods. TRAP staining of osteoclast cultures demonstrated a significant decrease in the number of osteoclasts in cultures from WT- and OI Treg-transplanted OI mice as compared with PBS-transplanted OI mice, as evident in representative images of the wells (Figure 5C, top panel, middle panel) as well in the cumulative graph (Figure 5Di). A significant reduction in the length and the area of the osteoclasts were seen in WT- and OI Treg-transplanted OI mice (Figure 5Dii and 5Diii). The number of nuclei per osteoclast was also significantly decreased after both WT and OI Treg transplantation (Figure 5Div). There was also a significant reduction in the activity of osteoclasts obtained from WT- and OI Treg-transplanted OI mice as compared with PBS-transplanted OI mice, measured by the formation of resorption pits seen in the images (Figure 5C, bottom panel) and the cumulative graph (Figure 5Dv). There were no differences in any of the parameters between the WT and OI Treg transplantations. A significant reduction was also observed in the expression of osteoclast-specific genes, NFATc1 (Figure 5Ei), CTSK (Figure 5Eii), and TRAP (Figure 5Eiii) in both WT- and OI Treg-transplanted OI mice compared with PBS-transplanted OI mice. The expression of all three genes was significantly lower in OI Treg-transplanted OI mice osteoclasts as compared with WT Treg-transplanted OI mice osteoclasts (Figure 5Ei, 5Eii, and 5Eiii).

Toluidine blue staining of the tibial sections demonstrated an increase in the trabeculae after WT and OI Treg transplantation compared with PBS transplantation (Figure 5F; red arrows). Morphometric analysis (n = 7–9 mice per group) demonstrated a significant increase in the percentage of osteoblasts surface/bone surface (Ob.S/BS) after WT and OI Treg transplantations (Figure 5Gi). There was also a significant increase in the number of osteoblasts per bone perimeter (N.Ob/B.Pm; Figure 5Gii) as well as the number of osteoblasts per total area (N.Ob/T.Ar; Figure 5Giii) in WT- and OI-transplanted OI mice as compared with PBS-transplanted OI mice. Ob.S/BS and N.Ob/B.Pm was significantly higher, whereas N.Ob/T.Ar was significantly lower in OI Treg-transplanted OI mice as compared with WT Treg-transplanted OI mice (Figure 5Gi , ii, iii). Week 3 osteoblastic cultures from calvaria and long bone demonstrates increased calcium deposition in WT- as well as OI Treg-transplanted OI mice as compared with PBS-transplanted OI mice, observed by increased alizarin red staining (Figure 5H). This increase in calcium deposition after transplantation is significant, as evident by the representative images of alizarin red staining of the entire well (Figure 5Ii) as well in the cumulative graph (Figure 5Iii). There was no difference between the calcium deposition seen after WT and OI Treg transplantation. Runx-2 mRNA expression levels showed a significant increase after WT Treg transplantation at weeks 1, 2, and 3, whereas there was no change after OI Treg transplantation (Figure 5Ji). Runx-2 expression was significantly lower in OI Treg-transplanted mice osteoblasts as compared with WT Treg-transplanted mice osteoblasts at all time points (Figure 5Ji). Alkaline phosphatase expression levels were significantly increased after WT Treg transplantation in weeks 1, 2, and 3, whereas OI Treg-transplanted osteoblasts showed a significant increase in alkaline phosphatase levels in weeks 2 and 3 (Figure 5Jii). Consequently, the alkaline phosphatase levels were significantly lower in OI Treg-transplanted osteoblasts compared with WT Treg-transplanted mice osteoblasts in week 1, but no change was seen in weeks 2 and 3 (Figure 5Jii). Osteocalcin mRNA expression levels were significantly higher in both WT- and OI Treg-transplanted mice osteoblasts as compared with PBS-transplanted OI mice osteoblasts at all time points studied (Figure 5Jiii). There was no difference in the levels in OI Treg-transplanted mice osteoblasts compared with WT Treg-transplanted mice osteoblasts in weeks 1 and 3, but in week 2, osteocalcin levels were significantly higher in OI transplanted mice osteoblasts when compared with WT Treg-transplanted osteoblasts (Figure 5Jiii).

These data indicate that transplantation of WT and OI Tregs can reduce osteoclast number and activity as well as increase osteoblast number and calcium deposition, which can then induce the clinical improvements seen in the OI mice after transplantation. Moreover, in most parameters studied, transplantation of OI Tregs brings about enhanced progression than transplantation of WT Tregs.

DISCUSSION

The results in this study provide evidence that a pro-inflammatory environment exists in OI owing to a quantitative decrease in tolerance-inducing Tregs with an anti-inflammatory signature, which also contributes to the activated effector T cell phenotype. Importantly, restoring the Tregs dampened this pro-inflammatory environment and enhanced bone morphometric parameters and strength owing to reduced osteoclast number and increased osteoblast mineralization. There are no previous reports on T cells' or Tregs' role in bone remodeling in OI; thus, the presented results provide an opportunity for adoptive Treg transfer to alleviate OI symptoms in the future.

OI is a rare skeletal dysplasia that affects one in 20,000 births. Clinically and genetically highly heterogeneous, it is characterized by a decreased bone mass and altered microarchitecture that results in an increased bone fragility leading to frequent fractures (Rauch and Glorieux, 2004). OI is usually caused by autosomal dominant mutations in genes encoding procollagen alpha chains (COL1α1/COL1α2), which may cause defects in collagen quantity (a milder form of OI) or collagen quality owing to the abnormal assembly of the protein (moderate-to-severe-to-lethal forms of OI) (Marini et al., 2017). Other severe OI forms are owing to recessive mutations in non-collagenous genes that affect collagen post-translational modifications, bone matrix mineralization, osteoblast differentiation, and function (Kang et al., 2017). For all different OI forms, several other therapies are currently being used for treatment.

Recent reports have suggested that pediatric OI patients present hyperinflammed conditions with increased platelet counts (Salter et al., 2018). Similarly, in a cohort of patients with type V OI, the formation of hyperplastic callus (a distinctive clinical manifestation of this type of OI) was associated with increased erythrocyte sedimentation rate and levels of C-reactive protein (Cao et al., 2019). Other studies have also shown potential activation of inflammatory pathways (Rauch et al., 2018) and increased serum levels of TNF-α, suggesting chronic inflammation (Matthews et al., 2017). Considering these previous reports, we initiated the analysis of T cell subsets in the OI mice and report that OI mice exhibit an activated T cell phenotype with increased ability to secrete inflammatory cytokines, IFN-γ and TNF-α. Thus, there exists a pro-inflammatory environment in the OI mouse. Previous studies have shown that inflammation can lead to excessive bone resorption, owing to upregulation or hyperactivity of osteoclasts and impaired bone formation, owing to downregulation or hypoactivity of osteoblasts (Mundy, 2007; Redlich and Smolen, 2012; Romas and Gillespie, 2006). Even though there exists a state of high bone turnover in OI (Kalajzic et al., 2002), it has been shown that the high rate of bone formation cannot compensate for the much higher rate of bone resorption owing to the increased formation and activity of osteoclasts (Kalajzic et al., 2002; Li et al., 2010). It may be possible that the hyperactivity of the osteoclasts seen in OI may be exaggerated as a result of the pro-inflammatory conditions that exist as activated T cells express receptor activator of NF-κB Ligand (RANKL), which plays a critical role in the regulation of osteoclastogenesis (Wang et al., 2002).

On examining the reason for the pro-inflammatory environment observed in the OI mice, our data demonstrated a quantitative decrease in the number of Tregs in the OI mice, even though their functional activity was the same when compared with WT mice. Physiologically, Tregs are a specialized subpopulation of T cells that keep the immune response in check by inducing tolerance (Kondelkova et al., 2010). Thus, the T cells' activated phenotype observed in OI inversely correlates with the number of Tregs. However, it is not entirely clear why the number of Tregs is decreased in a genetic disease that has mutated or reduced collagen. However, clues can be taken from the studies that show that treating naive T cells with collagen-derived peptides promoted the development and differentiation of Tregs *in vitro* (Nishikimi et al., 2018), and feeding mice with polymerized-type I collagen upregulated Treg differentiation *in vivo* in mice model of early and established arthritis (Furuzawa-Carballeda et al., 2012). Thus, decreased or mutated collagen can influence the development of the Tregs from CD4$^+$ T cells.

Furthermore, several cytokines are essential for developing Tregs, the most important being TGF-β and IL-2 (Toomer and Malek, 2018). It has been shown that excessive TGF-β signaling is a common mechanism in both recessive (Crtap$^{-/-}$) and dominant (Col1a2$^{tm1.1Mcbn}$) OI mouse models (Grafe et al., 2014). However,

the tissues studied in this study were the skeletal tissues and lungs. Our data show that TGF-β receptor I and II expression was significantly reduced in splenic T cells from OI mice compared with WT mice (Figure S3). Despite the high levels of TGF-β in OI, its signaling is likely dampened and leads to reduced generation and maintenance of Tregs.

Tregs have been shown to affect the osteoclasts and the osteoblasts directly. Treg cells' accumulation at sites of the epiphysis of long bones, where bone highly remodels, favors the concept that Treg cells can act locally on the bone (Bozec and Zaiss, 2017). Treg can interfere with bone resorption by affecting osteoclast development and function (Bozec and Zaiss, 2017; Fischer et al., 2019). Some studies have identified inhibitory cytokines as critical players in Treg cell-mediated suppression of osteoclasts (Kim et al., 2007); other reports suggested cell-cell-contact dependent mechanisms (Zaiss et al., 2007). Our data show that conditioned media from Tregs (both from WT and OI mice) significantly reduced osteoclasts' formation *in vitro* in OI bone marrow cell cultures, indicating Tregs' effects on OI are dependent on the inhibitory cytokines. Tregs can inhibit osteoclast formation via cytokines such as IL-10 and TGF-β (Luo et al., 2011). The role and the nature of the cytokines involved, the stage of osteoclastogenesis where the inhibition occurs, and the mechanism of the inhibition in OI can be the focus of future studies. Tregs may also directly interact with bone-forming cells, osteoblasts, or their progenitor cells (Lei et al., 2015). However, the effect of Treg on osteoblasts is under-investigated. A couple of studies have shown that PTH exerts its bone anabolic activity by increasing the number of Tregs. The blockade of Treg increase was also shown to hamper bone formation and trabecular bone volume and structure induced by PTH (Yu et al., 2018). The same group further shows that butyrate, a metabolite that causes Tregs' expansion (Arpaia et al., 2013), regulates bone anabolism via Treg-mediated regulation of CD8$^+$ T cell production of the osteogenic factor Wnt10b (Tyagi et al., 2018).

Furthermore, it has been implicated that Tregs play a role in bone formation by promoting the proliferation and differentiation of osteoblasts directly (Lei et al., 2015) by secreting cytokines and activating downstream effectors that induce mesenchymal stem cells to differentiate into osteoblasts (Zhu et al., 2020). Our data demonstrate that conditioned media from both WT and OI Tregs augments the differentiation of cultured osteoblasts from OI mice (a model with high turnover) as it significantly increases the calcium deposition. The factors secreted by Tregs that play a role and the mechanisms involved in OI's osteoblastic differentiation will be determined in future studies.

Treg transplantation has gained widespread attention as Tregs offer a new therapeutic option for controlling undesired systemic and local immune responses (Pappritz et al., 2018) and has been used as a therapy for various diseases (Bayry and Gautier, 2016; Bluestone et al., 2015; Gliwinski et al., 2017; Tang and Vincenti, 2017). It has been shown that the adoptive transfer of Tregs can bring about enhanced bone healing in an osteotomy model (Schlundt et al., 2019). A reduction in the levels of IFN-γ and TNF-α by systemic infusion of Tregs markedly improved bone marrow mesenchymal stromal cells-based bone regeneration and calvarial defect repair (Liu et al., 2011). Furthermore, systemic infusion of bone marrow mesenchymal stromal cells significantly enhanced the repair of critical-sized calvarial defects via Tregs' upregulation (Liu et al., 2015). In a canine model of periodontitis, it has been shown that Tregs are recruited to the site of the injury and decrease bone resorption by reducing inflammation (Glowacki et al., 2013). Moreover, CD4$^+$CD25$^+$ T cells' adoptive transfer into T cell-deficient RAG-1 knockout mice increased the bone mass in these mice, indicating that Tregs probably can directly affect bone homeostasis without the need to engage other T cell lineages.

Our data now show that the systemic transplantation of Tregs into OI mice resulted in a significantly enhanced improvement in tibial trabecular and cortical parameters and an increase in the stiffness of the femur. We also demonstrate that Treg transplantation resulted in decreased T cell activation and a decrease in the effector cytokines IFN-γ and TNF-α. Furthermore, an increase in mineralization of osteoblasts and a reduction in osteoclast number were observed in cells from Treg-transplanted OI mice. Thus, Treg transplantation can have beneficial effects on OI. In addition, we also demonstrate that transplantation of OI Tregs caused the same outcomes as seen with the transplantation of WT Tregs. This finding is particularly significant for future clinical trials where OI patients' peripheral T cells are used to *ex vivo* program to iTregs and then transplanted back into the same individual. Our longitudinal micro-CT data do show that the positive effects seem to decline at six months after transplantation, more so with WT Treg transplantation than with OI Treg transplantation. Therefore, repeated transplantations with Tregs might

be required. Nonetheless, this study's pre-clinical data demonstrate that Treg transplantation could be a viable option for OI therapy. We believe that further determining the efficacy of cellular therapy with Tregs will be significant in opening up future translational avenues of non-toxic autologous therapy for OI patients.

Limitations of the study

This study establishes that owing to the lower number of suppressive Tregs in OI, there exists an activated phenotype of T cells with increased levels of pro-inflammatory cytokines. We also show that restoring Treg numbers could modulate the disease outcome. However, this study does not establish the underlying mechanism for reduced Treg numbers in a genetic disease owing to collagen mutation. Similarly, we observed an increase in osteoblast differentiation and a decrease in osteoclast numbers, but this study does not examine the mechanisms by which an increase in Treg numbers can bring about these changes in OI. All these questions would form the basis of future studies.

DATA AND MATERIAL AVAILABILITY

All data generated or analyzed during this study are included in this paper.

STAR★METHODS

Detailed methods are provided in the online version of this paper and include the following:

- KEY RESOURCES TABLE
- RESOURCE AVAILABILITY
  - Lead contact
  - Materials availability
  - Data and code availability
- EXPERIMENTAL MODEL AND SUBJECT DETAILS
  - Mice
- METHOD DETAILS
  - Study design
  - T cell isolation
  - Induced treg (iTreg) differentiation
  - T cell suppression assay
  - Flow cytometry
  - Cytokine measurement by ELISA
  - Real-time qPCR
  - Transplantation
  - Micro-CT analysis
  - Mechanical testing
  - Bone histomorphometry
  - Osteoblast cell culture
  - Alizarin red staining
  - Osteoclast cell culture
- TARTRATE-RESISTANT ACID PHOSPHATASE (TRAP) STAINING
- BONE RESORPTION ASSAY
  - Microscopy
- QUANTIFICATION AND STATISTICAL ANALYSIS

SUPPLEMENTAL INFORMATION

Supplemental information can be found online at https://doi.org/10.1016/j.isci.2022.104818.

AUTHOR CONTRIBUTIONS

I.-H.K.: conception and design, collection and assembly of data, data analysis and interpretation, manuscript writing.

U.K.B.: collection and assembly of data, data analysis, and interpretation.

S.C.: collection and assembly of data, data analysis, and interpretation.

P.C.: collection and assembly of data, data analysis, and interpretation.

S.C.: collection and assembly of data, data analysis, and interpretation.

N.B.: collection and assembly of data, data analysis, and interpretation.

H.L.: data analysis and interpretation.

Y.W.: collection and assembly of data, data analysis, and interpretation.

H.Y.: data analysis and interpretation, critical reading, and final approval of the manuscript.

S.M.: data analysis and interpretation, critical reading, and final approval of the manuscript.

M.M.: conception and design, collection and assembly of data, data analysis and interpretation, manuscript writing, financial support, final approval of the manuscript.

DECLARATION OF INTERESTS

The authors declare no competing interests and no potential conflicts of interest concerning this paper's authorship or publication. None of the data in this paper has been published, nor is it in consideration to be published elsewhere. A US patent #16/772,967, related to the use of Treg transplantation in OI, has been applied on June 15, 2020 and we are awaiting a decision.

INCLUSION AND DIVERSITY STATEMENT

We worked to ensure sex balance in the selection of non-human subjects. The author list of this paper includes contributors from the location where the research was conducted who participated in the data collection, design, analysis, and/or interpretation of the work.

REFERENCES

Arpaia, N., Campbell, C., Fan, X., Dikiy, S., van der Veeken, J., deRoos, P., Liu, H., Cross, J.R., Pfeffer, K., Coffer, P.J., and Rudensky, A.Y. (2013). Metabolites produced by commensal bacteria promote peripheral regulatory T-cell generation. Nature 504, 451–455.

Baaten, B.J., Li, C.R., and Bradley, L.M. (2010a). Multifaceted regulation of T cells by CD44. Commun. Integr. Biol. 3, 508–512.

Baaten, B.J.G., Li, C.R., Deiro, M.F., Lin, M.M., Linton, P.J., and Bradley, L.M. (2010b). CD44 regulates survival and memory development in Th1 cells. Immunity 32, 104–115.

Baaten, B.J.G., Tinoco, R., Chen, A.T., and Bradley, L.M. (2012). Regulation of antigen-experienced T cells: lessons from the quintessential memory marker CD44. Front. Immunol. 3, 23.

Bayry, J., and Gautier, J.F. (2016). Regulatory T cell immunotherapy for type 1 diabetes: a step closer to success? Cell Metab. 23, 231–233.

Bluestone, J.A., Buckner, J.H., Fitch, M., Gitelman, S.E., Gupta, S., Hellerstein, M.K., Herold, K.C., Lares, A., Lee, M.R., Li, K., et al. (2015). Type 1 diabetes immunotherapy using polyclonal regulatory T cells. Sci. Transl. Med. 7, 315ra189.

Boone, J.M., Velazquez, O., and Cherry, S.R. (2004). Small-animal X-ray dose from micro-CT. Mol. Imaging 3, 149–158.

Bouxsein, M.L., Boyd, S.K., Christiansen, B.A., Guldberg, R.E., Jepsen, K.J., and Müller, R. (2010). Guidelines for assessment of bone microstructure in rodents using micro-computed tomography. J. Bone. Miner. Res. 25, 1468–1486.

Bozec, A., and Zaiss, M.M. (2017). T regulatory cells in bone remodelling. Curr. Osteoporos. Rep. 15, 121–125.

Cao, Y.J., Wei, Z., Zhang, H., and Zhang, Z.L. (2019). Expanding the clinical spectrum of osteogenesis imperfecta type V: 13 additional patients and review. Front. Endocrinol. 10, 375.

Caramalho, Í., Nunes-Cabaço, H., Foxall, R.B., and Sousa, A.E. (2015). Regulatory T-cell development in the human thymus. Front. Immunol. 6, 395.

Chatterjee, S., Eby, J.M., Al-Khami, A.A., Soloshchenko, M., Kang, H.K., Kaur, N., Naga, O.S., Murali, A., Nishimura, M.I., Caroline Le Poole, I., and Mehrotra, S. (2014). A quantitative increase in regulatory T cells controls development of vitiligo. J. Invest. Dermatol. 134, 1285–1294.

Chipman, S.D., Sweet, H.O., McBride, D.J., Jr., Davisson, M.T., Marks, S.C., Jr., Shuldiner, A.R., Wenstrup, R.J., Rowe, D.W., and Shapiro, J.R. (1993). Defective pro alpha 2(I) collagen synthesis in a recessive mutation in mice: a model of human osteogenesis imperfecta. Proc. Natl. Acad. Sci. USA 90, 1701–1705.

Cibrián, D., and Sánchez-Madrid, F. (2017). CD69: from activation marker to metabolic gatekeeper. Eur. J. Immunol. 47, 946–953.

Fischer, L., Herkner, C., Kitte, R., Dohnke, S., Riewaldt, J., Kretschmer, K., and Garbe, A.I. (2019). Foxp3(+) regulatory T cells in bone and hematopoietic homeostasis. Front. Endocrinol. 10, 578.

Furuzawa-Carballeda, J., Macip-Rodriguez, P., Galindo-Feria, A.S., Cruz-Robles, D., Soto-Abraham, V., Escobar-Hernandez, S., Aguilar, D., Alpizar-Rodriguez, D., Ferez-Blando, K., and Llorente, L. (2012). Polymerized-type I collagen induces upregulation of Foxp3-expressing CD4 regulatory T cells and downregulation of IL-17-producing CD4(+) T cells (Th17) cells in collagen-induced arthritis. Clin. Dev. Immunol. 2012, 618608.

Gliwiński, M., Iwaszkiewicz-Grześ, D., and Trzonkowski, P. (2017). Cell-based therapies with T regulatory cells. BioDrugs 31, 335–347.

Glowacki, A.J., Yoshizawa, S., Jhunjhunwala, S., Vieira, A.E., Garlet, G.P., Sfeir, C., and Little, S.R. (2013). Prevention of inflammation-mediated bone loss in murine and canine periodontal disease via recruitment of regulatory lymphocytes. Proc. Natl. Acad. Sci. USA 110, 18525–18530.

Grafe, I., Yang, T., Alexander, S., Homan, E.P., Lietman, C., Jiang, M.M., Bertin, T., Munivez, E., Chen, Y., Dawson, B., et al. (2014). Excessive transforming growth factor-beta signaling is a common mechanism in osteogenesis imperfecta. Nat. Med. 20, 670–675.

Kalajzic, I., Terzic, J., Rumboldt, Z., Mack, K., Naprta, A., Ledgard, F., Gronowicz, G., Clark, S.H., and Rowe, D.W. (2002). Osteoblastic response to the defective matrix in the osteogenesis imperfecta murine (oim) mouse. Endocrinology 143, 1594–1601.

Kang, H., Aryal A C, S., and Marini, J.C. (2017). Osteogenesis imperfecta: new genes reveal novel mechanisms in bone dysplasia. Transl. Res. 181, 27–48.

Kim, Y.G., Lee, C.K., Nah, S.S., Mun, S.H., Yoo, B., and Moon, H.B. (2007). Human CD4+CD25+ regulatory T cells inhibit the differentiation of osteoclasts from peripheral blood mononuclear cells. Biochem. Biophys. Res. Commun. 357, 1046–1052.

Kondělková, K., Vokurková, D., Krejsek, J., Borská, L., Fiala, Z., and Ctirad, A. (2010). Regulatory T cells (TREG) and their roles in immune system with respect to immunopathological disorders. Acta. Medica. 53, 73–77.

Kong, Y.Y., Feige, U., Sarosi, I., Bolon, B., Tafuri, A., Morony, S., Capparelli, C., Li, J., Elliott, R., McCabe, S., et al. (1999). Activated T cells regulate bone loss and joint destruction in adjuvant arthritis through osteoprotegerin ligand. Nature 402, 304–309.

Könnecke, I., Serra, A., El Khassawna, T., Schlundt, C., Schell, H., Hauser, A., Ellinghaus, A., Volk, H.D., Radbruch, A., Duda, G.N., and Schmidt-Bleek, K. (2014). T and B cells participate in bone repair by infiltrating the fracture callus in a two-wave fashion. Bone 64, 155–165.

Lee, W., and Lee, G.R. (2018). Transcriptional regulation and development of regulatory T cells. Exp. Mol. Med. 50, e456.

Lei, H., Schmidt-Bleek, K., Dienelt, A., Reinke, P., and Volk, H.D. (2015). Regulatory T cell-mediated anti-inflammatory effects promote successful tissue repair in both indirect and direct manners. Front. Pharmacol. 6, 184.

Li, H., Jiang, X., Delaney, J., Franceschetti, T., Bilic-Curcic, I., Kalinovsky, J., Lorenzo, J.A., Grcevic, D., Rowe, D.W., and Kalajzic, I. (2010). Immature osteoblast lineage cells increase osteoclastogenesis in osteogenesis imperfecta murine. Am. J. Pathol. 176, 2405–2413.

Liu, Y., Wang, L., Kikuiri, T., Akiyama, K., Chen, C., Xu, X., Yang, R., Chen, W., Wang, S., and Shi, S. (2011). Mesenchymal stem cell-based tissue regeneration is governed by recipient T lymphocytes via IFN-gamma and TNF-alpha. Nat. Med. 17, 1594–1601.

Liu, Y., Yang, R., and Shi, S. (2015). Systemic infusion of mesenchymal stem cells improves cell-based bone regeneration via upregulation of regulatory T cells. Tissue Eng. Part A 21, 498–509.

Luo, C.Y., Wang, L., Sun, C., and Li, D.J. (2011). Estrogen enhances the functions of CD4(+) CD25(+)Foxp3(+) regulatory T cells that suppress osteoclast differentiation and bone resorption in vitro. Cell. Mol. Immunol. 8, 50–58.

Marini, J.C., Forlino, A., Bächinger, H.P., Bishop, N.J., Byers, P.H., Paepe, A.D., Fassier, F., Fratzl-Zelman, N., Kozloff, K.M., Krakow, D., et al. (2017). Osteogenesis imperfecta. Nat. Rev. Dis. Primers 3, 17052.

Matthews, B.G., Roeder, E., Wang, X., Aguila, H.L., Lee, S.K., Grcevic, D., and Kalajzic, I. (2017). Splenomegaly, myeloid lineage expansion and increased osteoclastogenesis in osteogenesis imperfecta murine. Bone 103, 1–11.

Mucida, D., Park, Y., Kim, G., Turovskaya, O., Scott, I., Kronenberg, M., and Cheroutre, H. (2007). Reciprocal TH17 and regulatory T cell differentiation mediated by retinoic acid. Science 317, 256–260.

Mundy, G.R. (2007). Osteoporosis and inflammation. Nutr. Rev. 65, S147–S151.

Nam, D., Mau, E., Wang, Y., Wright, D., Silkstone, D., Whetstone, H., Whyne, C., and Alman, B. (2012). T-lymphocytes enable osteoblast maturation via IL-17F during the early phase of fracture repair. PLoS One 7, e40044.

Nishikimi, A., Koyama, Y.I., Ishihara, S., Kobayashi, S., Tometsuka, C., Kusubata, M., Kuwaba, K., Hayashida, O., Hattori, S., and Katagiri, K. (2018). Collagen-derived peptides modulate CD4(+) T-cell differentiation and suppress allergic responses in mice. Immun. Inflamm. Dis. 6, 245–255.

Pappritz, K., Savvatis, K., Miteva, K., Kerim, B., Dong, F., Fechner, H., Müller, I., Brandt, C., Lopez, B., González, A., et al. (2018). Immunomodulation by adoptive regulatory T-cell transfer improves Coxsackievirus B3-induced myocarditis. FASEB j. 32, 6066–6078.

Parfitt, A.M., Drezner, M.K., Glorieux, F.H., Kanis, J.A., Malluche, H., Meunier, P.J., Ott, S.M., and Recker, R.R. (1987). Bone histomorphometry: standardization of nomenclature, symbols, and units. Report of the ASBMR Histomorphometry Nomenclature Committee. J. Bone. Miner. Res. 2, 595–610.

Rauch, F., Geng, Y., Lamplugh, L., Hekmatnejad, B., Gaumond, M.H., Penney, J., Yamanaka, Y., and Moffatt, P. (2018). Crispr-Cas9 engineered osteogenesis imperfecta type V leads to severe skeletal deformities and perinatal lethality in mice. Bone 107, 131–142.

Rauch, F., and Glorieux, F.H. (2004). Osteogenesis imperfecta. Lancet 363, 1377–1385.

Redlich, K., and Smolen, J.S. (2012). Inflammatory bone loss: pathogenesis and therapeutic intervention. Nat. Rev. Drug. Discov. 11, 234–250.

Reinke, S., Geissler, S., Taylor, W.R., Schmidt-Bleek, K., Juelke, K., Schwachmeyer, V., Dahne, M., Hartwig, T., Akyüz, L., Meisel, C., et al. (2013). Terminally differentiated CD8(+) T cells negatively affect bone regeneration in humans. Sci. Transl. Med. 5, 177ra36. 177ra136.

Romas, E., and Gillespie, M.T. (2006). Inflammation-induced bone loss: can it be prevented? Rheum. Dis. Clin. North. Am. 32, 759–773.

Sakaguchi, S., Sakaguchi, N., Asano, M., Itoh, M., and Toda, M. (1995). Immunologic self-tolerance maintained by activated T cells expressing IL-2 receptor alpha-chains (CD25). Breakdown of a single mechanism of self-tolerance causes various autoimmune diseases. J. Immunol. 155, 1151–1164.

Salter, L., Offiah, A.C., and Bishop, N. (2018). Elevated platelet counts in a cohort of children with moderate-severe osteogenesis imperfecta suggest that inflammation is present. Arch. Dis. Child. 103, 767–771.

Schlundt, C., Reinke, S., Geissler, S., Bucher, C.H., Giannini, C., Märdian, S., Dahne, M., Kleber, C., Samans, B., Baron, U., et al. (2019). Individual effector/regulator T cell ratios impact bone regeneration. Front. Immunol. 10, 1954.

Schmidt, A., Eriksson, M., Shang, M.M., Weyd, H., and Tegnér, J. (2016). Comparative analysis of

protocols to induce human CD4+Foxp3+ regulatory T cells by combinations of IL-2, TGF-beta, retinoic acid, rapamycin and butyrate. PLoS One 11, e0148474.

Shapiro, J.R., McBride, D.J., Jr., and Fedarko, N.S. (1995). OIM and related animal models of osteogenesis imperfecta. Connect. Tissue. Res. 31, 265–268.

Takayanagi, H. (2015). Osteoimmunology in 2014: two-faced immunology-from osteogenesis to bone resorption. Nat. Rev. Rheumatol. 11, 74–76.

Talaat, R.M., Sidek, A., Mosalem, A., and Kholief, A. (2015). Effect of bisphosphonates treatment on cytokine imbalance between TH17 and Treg in osteoporosis. Inflammopharmacology 23, 119–125.

Tang, Q., and Bluestone, J.A. (2013). Regulatory T-cell therapy in transplantation: moving to the clinic. Cold Spring Harb. Perspect. Med. 3, a015552.

Tang, Q., and Vincenti, F. (2017). Transplant trials with Tregs: perils and promises. J. Clin. Invest. 127, 2505–2512.

Thomas, I.H., and DiMeglio, L.A. (2016). Advances in the classification and treatment of osteogenesis imperfecta. Curr. Osteoporos. Rep. 14, 1–9.

Toben, D., Schroeder, I., El Khassawna, T., Mehta, M., Hoffmann, J.E., Frisch, J.T., Schell, H., Lienau, J., Serra, A., Radbruch, A., and Duda, G.N. (2011). Fracture healing is accelerated in the absence of the adaptive immune system. J. Bone. Miner. Res. 26, 113–124.

Toomer, K.H., and Malek, T.R. (2018). Cytokine signaling in the development and homeostasis of regulatory T cells. Cold Spring Harb. Perspect. Biol. 10, a028597.

Tyagi, A.M., Yu, M., Darby, T.M., Vaccaro, C., Li, J.Y., Owens, J.A., Hsu, E., Adams, J., Weitzmann, M.N., Jones, R.M., and Pacifici, R. (2018). The microbial metabolite butyrate stimulates bone formation via T regulatory cell-mediated regulation of WNT10B expression. Immunity 49, 1116–1131.e7. e1117.

Uveges, T.E., Kozloff, K.M., Ty, J.M., Ledgard, F., Raggio, C.L., Gronowicz, G., Goldstein, S.A., and Marini, J.C. (2009). Alendronate treatment of the

brtl osteogenesis imperfecta mouse improves femoral geometry and load response before fracture but decreases predicted material properties and has detrimental effects on osteoblasts and bone formation. J. Bone. Miner. Res. 24, 849–859.

Wang, R., Zhang, L., Zhang, X., Moreno, J., Celluzzi, C., Tondravi, M., and Shi, Y. (2002). Regulation of activation-induced receptor activator of NF-kappaB ligand (RANKL) expression in T cells. Eur. J. Immunol. 32, 1090–1098.

Weitzmann, M.N., and Pacifici, R. (2005). The role of T lymphocytes in bone metabolism. Immunol. Rev. 208, 154–168.

Xiao, S., Jin, H., Korn, T., Liu, S.M., Oukka, M., Lim, B., and Kuchroo, V.K. (2008). Retinoic acid increases Foxp3+ regulatory T cells and inhibits development of Th17 cells by enhancing TGF-beta-driven Smad3 signaling and inhibiting IL-6 and IL-23 receptor expression. J. Immunol. 181, 2277–2284.

Yu, M., D'Amelio, P., Tyagi, A.M., Vaccaro, C., Li, J.Y., Hsu, E., Buondonno, I., Sassi, F., Adams, J., Weitzmann, M.N., et al. (2018). Regulatory T cells are expanded by Teriparatide treatment in humans and mediate intermittent PTH-induced bone anabolism in mice. EMBO. Rep. 19, 156–171.

Zaiss, M.M., Axmann, R., Zwerina, J., Polzer, K., Gückel, E., Skapenko, A., Schulze-Koops, H., Horwood, N., Cope, A., and Schett, G. (2007). Treg cells suppress osteoclast formation: a new link between the immune system and bone. Arthritis. Rheum. 56, 4104–4112.

Zaiss, M.M., Sarter, K., Hess, A., Engelke, K., Böhm, C., Nimmerjahn, F., Voll, R., Schett, G., and David, J.P. (2010). Increased bone density and resistance to ovariectomy-induced bone loss in FoxP3-transgenic mice based on impaired osteoclast differentiation. Arthritis Rheum. 62, 2328–2338.

Zhu, L., Hua, F., Ding, W., Ding, K., Zhang, Y., and Xu, C. (2020). The correlation between the Th17/Treg cell balance and bone health. Immun. Ageing 17, 30.

Ziegler, S.F., Ramsdell, F., and Alderson, M.R. (1994). The activation antigen CD69. Stem. Cell. 12, 456–465.

STAR★METHODS

KEY RESOURCES TABLE

REAGENT or RESOURCE	SOURCE	IDENTIFIER
Antibodies		
Anti-mouse CD3	BioXCell	Clone:145–2C11; Cat#BE0001–1; RRID:AB_1107634
Anti-mouse CD28	BioXCell	Clone:37.51; Cat#BE0015–1; RRID:AB_1107624
Anti-mouse FoxP3-PE	eBioscience	Clone:FJK-16s; Cat#12-5773-82
Anti-mouse CD4-PE/Cy7	Biolegend	Clone:GK5.1; Cat#100422; RRID:AB_312707
Anti-mouse CD4-APC	Biolegend	Clone:GK5.1; Cat#100412; RRID:AB_312697
Anti-mouse CD44-APC	Biolegend	Clone; IM7; Cat#103012; RRID:AB_312963
Anti-mouse IFN-γ-PE	Biolegend	Clone: XMG1.2; Cat#505808; RRID:AB_315402
Anti-mouse TNF-α-PE/Cy7	Biolegend	Clone: MP6-XT22; Cat#506306; RRID:AB_315427
Anti-mouse CD69-PE	Biolegend	Clone: H1.F3; Cat#104508; RRID:AB_313111
Anti-mouse TGF-β	Biolegend	Cat#580702
Anti-mouse CD8-BV510	Biolegend	Clone: 53–6.7; Cat#100752; RRID:AB_2563057
Biotinylated anti-mouse CD19	Biolegend	Cat#101504; RRID:AB_312823
Biotinylated anti-mouse CD11b	Biolegend	Cat#101204; RRID:AB_312787
Biotinylated anti-mouse CD11c	Biolegend	Cat# 117304; RRID:AB_313773
Biotinylated anti-mouse NK1.1	Biolegend	Cat# 108704; RRID:AB_313391
Biotinylated anti-mouse CD25	Biolegend	Cat# 102004; RRID:AB_312853
Chemicals, peptides, and recombinant proteins		
Streptavidin magnetic beads	BD Biosciences	Cat#557812
IL-2	Frederick National Laboratory for Cancer research	Tecin(teceleukin); Ro 23-6019
Retinoic acid	Sigma	Cat# R2625-50MG
RANKL	R&D Systems	Cat# 462-TEC-010
M-CSF		Cat# 576,404
Collagenase-P	Roche Diagnostic Corporation	Cat#11249002001
IMDM media	Hyclone	Cat#SH30228.01
Alpha-MEM	Gibco	Cat#12571-048
Fetal Calf Serum	AtlantaBiologicals	Cat#S11150
Fetal Bovine Serum	Gibco	Cat#26140-079
L-glutamine	Sigma	Catalog #G8540-100G
Penicillin/Streptomycin	AtlantaBiologicals	Catalog #B21210
Beta-mercaptoethanol	Thermo Scientific	Catalog # 35602
Ascorbic acid 2-phosphate	Wako Pure Chemical Industry	Cat# O19-12063
β-glycerophosphate	Sigma	Cat# 157241
PMA	Sigma	Cat# P8039-1MG
Ionomycin	Sigma	Cat# I0634-1MG
GolgiPlug™	BD Biosciences	Cat# 555029
Carboxyfluorescein Diacetate Succinimidyl Ester (CFSE)	Molecular Probes; Invitrogen	Cat# C1157
BD Cytofix/Cytoperm Kit	BD Biosciences	Cat# 554714
Trizol	Life Technologies	Cat# 15596026
iScript cDNA Synthesis Kit	BioRad	Cat#1725035

Continued

REAGENT or RESOURCE	SOURCE	IDENTIFIER
TaqMan Gene Expression Assay NFATc1	Thermo Fisher	Cat#4453320; Mm00479445_m1
TaqMan Gene Expression Assay CTSK	Thermo Fisher	Cat#4453320; Mm00484039_m1
TaqMan Gene Expression Assay TRAP	Thermo Fisher	Cat#4453320; Mm00475698_m1
TaqMan Gene Expression Assay Runx-2	Thermo Fisher	Cat#4453320; Mm00501584_m1
TaqMan Gene Expression Assay ALP	Thermo Fisher	Cat#4453320; Mm00475834_m1
TaqMan Gene Expression Assay Osteocalcin	Thermo Fisher	Cat#4453320; Mm03413826_mH
TaqMan Gene Expression Assay TGF-β receptor I	Thermo Fisher	Cat#4453320; Mm00436964_m1
TaqMan Gene Expression Assay TGF-β receptor II	Thermo Fisher	Cat#4453320; Mm03024091_m1
TaqMan Gene Expression Assay β-Actin	Thermo Fisher	Cat#4453320; Mm02619580_g1
Neomycin	Sigma	Cat #N1876-100G
Cetylpyridinium chloride	Sigma	Cat# C0732-100G
Sodium phosphate	Sigma	Cat# 342483
Sodium hypochlorite	Sigma	Catalog # 7681-52-9
Critical commercial assays		
Mouse IFN-γ ELISA kit	Biolegend	Cat#430801
Mouse TNF-α ELISA kit	Biolegend	Cat#430901
Alizarin Red Staining Kit	EMD Millipore Corporation	Cat#3070121
Leukocyte acid phosphatase kit	Sigma Aldrich	Catalog #387A-1KIT
Bone Resorption Kit	CosmoBio	Cat# CSR-BRA-48X2KIT
Experimental models: Organisms/strains		
oim/oim (B6C3Fe-a/a-Col1a2oim/J)	Jackson Laboratory	Cat# 001815
FoxP3.GFP mice (C.Cg-Foxp3tm2Tch/J)	Jackson Laboratory	Cat#006769
C57Bl/6J mice	Jackson Laboratory	Cat#000664
Software and algorithms		
FlowJo Software	BD	https://www.flowjo.com/solutions/flowjo/downloads/
CT Bone Visualization and Analysis	Siemens Medical Solution Medical Solutions	https://sharedimaging.com/
Analyze 12.0 software for Micro-CT	AnalyzeDirect	https://analyzedirect.com/
Electro force system	EnduraTec	ELF3200
Bioquant OSTEO II software platform	Bioquant Image Analysis Corporation	https://bioquant.com/
GraphPad Prism 6.0 software	GraphPad software Inc.	https://www.graphpad.com/scientific-software/prism/
Other		
Irradiated mice diet	Tekland Global Diets	
Isofluorane	Piramal	Cat# NDC 66794-017-25

RESOURCE AVAILABILITY

Lead contact

Further information and requests for resources and reagents should be directed to and will be fulfilled by the lead contact, Dr. Meenal Mehrotra (mehrotra@musc.edu).

Materials availability

This study did not generate new unique reagents.

Data and code availability

- The data reported in this paper will be shared by the lead contact upon request.

- This paper does not report original code.

- Any additional information required to reanalyze the data reported in this paper is available from the lead contact upon request

EXPERIMENTAL MODEL AND SUBJECT DETAILS

Mice

Homozygous OI mice (*oim/oim*; B6C3Fe-a/a-Col1a2oim/J; Jackson Laboratory, Catalog # 001,815) were used for all the experiments and as recipients for transplantation (Chipman et al., 1993). This *oim* mutation arose spontaneously in 1985 and the underlying defect is a mutation in COL1A2, which results in an absence of COL1A2 in these mice. Instead of forming heterotrimers with COL1A1, homotrimers are formed which interferes with the integrity and quantity of the osteoid that accumulates in the bone. *Oim/oim* mice have a phenotype similar to human type III OI, including abnormal bone mineralization (brittleness of bones), decreased bone density, and fragile skeleton susceptible to fractures; however, mice live an average life span. Tregs were obtained from FoxP3.GFP mice (C.Cg-Foxp3^{tm2Tch}/J; Jackson Laboratory, Catalog #006769), C57Bl/6J mice (Jackson Laboratory, catalog #000664), and *oim/oim* mice. All mice were bred and maintained at the Animal Research Facilities of the Medical University of South Carolina at 21-25 °C temperature, 55-65% humidity and 12:12 days/night cycles. At the time of the experiments, animals were 6–12 weeks old and weighed 20-25g. Each mouse experiment included seven to nine mice per group. Age-matched recipient and donor mice of both genders were included and randomly assigned to groups. The percentage of males and females used as transplant recipients was 56 and 44%, respectively. This age group and both sexes of mice were chosen as OI is a disease of pediatric and adolescent age group and both males and females are equally affected. The endpoint was six months post-transplantation, which allowed for assessing clinical changes and T cell and Treg function. In transplantation experiments, exclusion criteria included unspecified death of animals or loss of more than 20% of body weight. Experiments were carried out in an unblinded fashion, and each mouse served as a biological replicate. Flow cytometric measurements were done with at least three technical replicates. All experimental protocols were approved and performed following the Medical University of South Carolina's relevant guidelines and regulations. All aspects of animal research have been approved and conducted per PHS Policy on Humane Care and Use of Laboratory Animals and the Institutional Animal Care and Use Committee of the Medical University of South Carolina.

METHOD DETAILS

Study design

This study was designed to establish the T cells and Tregs' status in OI mice and examine if Treg Transplantation can benefit OI. To explore this, we first analyzed the T cells from the spleen to examine their activation state and the expression of the effector cytokines in them. We also analyzed the number and function of Tregs in OI and the effect of Treg conditioned media on osteoclast number and osteoblast differentiation. Lastly, we transplanted OI mice with Tregs from WT and OI mice. We investigated the T cell activation and effector cytokine expression by flow cytometry and the improvements in bone architecture and mechanics by longitudinal and *ex vivo* micro-CT and three-point bending. The effect of Treg transplantation on osteoclast number and osteoblast differentiation was also examined.

T cell isolation

Splenocytes from WT and *oim/oim* mice were isolated by the standard protocol of mashing spleens and collecting single cells through a 70µM cell strainer. Cells were grown in IMDM media supplemented with 10% FCS, 4mM L-glutamine, 100 U/ml penicillin, 100 µg/mL streptomycin, 55 µM beta-mercaptoethanol under 5% CO_2, and atmospheric oxygen at 37 °C in a humidified incubator. To evaluate intracellular cytokines by flow cytometry, cells were re-stimulated either with PMA/ionomycin for 4 h or with plate-bound anti-CD3 (5 µg/mL) anti-CD28 (5 µg/mL) antibodies overnight, in the presence of Golgi inhibitors (1 µL of BD Biosciences GolgiPlug for every 1 mL (10^6 cells/ml) of cell culture (used for inhibiting the secretion of proteins). nTregs were examined by staining cells for CD4, CD25, and FoxP3 and acquiring and analyzing using flow cytometry and FlowJo software. The absolute number of Tregs was calculated based

on the total number of Tregs, the total number of lymphocytes, and the total number of splenocytes or thymocytes obtained.

Induced treg (iTreg) differentiation

Naive CD4$^+$CD25$^-$ T cells were purified from total splenocytes of 6–10-week-old WT and *oim/oim* mice by incubating the cells with biotinylated anti-CD19, anti-CD11b, anti-CD11c, anti-NK1.1, anti-CD25, followed by negative selection with streptavidin magnetic beads. For obtaining CD4$^+$ T cells from FoxP3.GFP mice and CD4$^+$GFP$^-$ cells were sorted from splenocytes using flow cytometry. The cells were cultured with 5 μg/ml anti-CD3, 5 μg/ml anti-CD28, 100u/ml IL-2, 5 ng/ml TGF-β and 40 nM/ml retinoic acid for 3 days (Chatterjee et al., 2014; Mucida et al., 2007; Schmidt et al., 2016; Xiao et al., 2008) to differentiate into iTregs. After three days, a cohort of cells was analyzed for FoxP3 expression by flow cytometry to determine the percentage and number of iTregs generated. Conditioned media was generated by incubating washed iTregs with serum-free media for 24 h, then collected, centrifuged, and stored at −80 °C until needed. Along with collecting Treg conditioned media, we also incubated the same amount of the serum-free media in an empty well and incubated for 24h. This was collected, centrifuged, and stored at −80 °C until needed and then used as the Control Media.

T cell suppression assay

T cell suppression assay, using Carboxyfluorescein Diacetate Succinimidyl Ester (CFSE) staining, was conducted in co-cultures of Tregs (sorted CD4$^+$CD25$^+$) from WT and *oim/oim* mice and 5-(and −6)-carboxyfluorescein diacetate succinimidyl ester (CFDA SE; Molecular Probes) labeled T cells (CD4$^+$CD25$^-$), from WT mice, at 1:1 and 1:2 ratios. Cells were grown for three days in the presence and absence of anti-CD3 and anti-CD28 antibodies and subsequently analyzed for CFSE using flow cytometry.

Flow cytometry

Staining for cell surface markers was performed by incubating cells with the appropriate antibody at 1:200 dilutions in PBS/0.1%BSA buffer. For intracellular cytokines, cells were fixed/permeabilized (BD Cytofix/Cytoperm Kit, BD Biosciences) before staining. For FoxP3, cells were fixed/permeabilized with FoxP3 staining buffer (eBioscience). Samples were acquired on BD LSRFortessa (BD Biosciences) and analyzed with FlowJo software.

Cytokine measurement by ELISA

Mouse IFN-γ and TNF-α ELISA kits were purchased from BioLegend, and ELISA was performed according to the manufacturer's protocol. Supernatants from CD4 and CD8 T cells from spleens of WT and OI mice and serum from WT and OI mice and PBS, WT, and OI Treg transplanted OI mice were collected and assayed using a standard curve generated by recombinant IFN-γ and TNF-α. The optical density of the samples was measured at 450 nm in a microplate reader, with the absorbance at 570 nm used as a reference and was subtracted from the absorbance at 450 nm. The data is calculated using a 4-parameter logistics curve-fitting algorithm.

Real-time qPCR

Total RNA was extracted from Splenocytes' pellets of WT and OI mice or OI mice transplanted with PBS, WT, and OI Tregs and from osteoclasts and osteoblasts from WT and OI Treg conditioned media treated cultures as well as cultures from PBS, WT, and OI Treg transplanted OI mice, using Trizol reagent (Life technologies). cDNA was generated from 1 μg total RNA using the iScript cDNA Synthesis Kit (BioRad). Quantitative real-time PCR was performed using a TaqMan Gene Expression Assays for TGF-β receptors I and II, Nuclear Factor of Activated T Cells 1 (NFATc1), Cathepsin K (CTSK), Tartrate-resistant Acid Phosphatase (TRAP), Runt-related Transcription Factor 2 (Runx-2), Alkaline Phosphatase and Osteocalcin and StepOne Real-time PCR System (Thermo Fisher). In addition, expression was quantified relative to β-Actin.

Transplantation

iTregs were generated as described above, and flow cytometry was performed to determine the percentage of iTregs (examining GFP expression in FoxP3.GFP mice and FoxP3 expression in *oim/oim* mice), which was on an average >85%. Cells were then suspended at 1.5×10^6/50ul in PBS and kept on ice until transplantation.

Twelve-week-old *oim/oim* mice were used as recipients. All recipient mice were scanned by micro-CT before transplantation to obtain baseline images. Recipient mice were given a single dose of total-body irradiation using a 4×10^6 V linear accelerator (300-cGy) and injected with cells via the tail vein. After transplantation, mice were injected with IL-2 intraperitoneally for three days to expand transplanted iTregs (Tang and Bluestone, 2013). Post-transplantation, mice were fed an irradiated diet (Tekland Global Diets) and MilliQ water with neomycin (200mg/300mL) added in the first month to prevent infection.

Micro-CT analysis

Longitudinal micro-CT is helpful as it allows the same animal to be followed over time, decreasing result variability and economizing mice (Bouxsein et al., 2010). Mice were imaged pre-transplantation for baseline and 2, 4, and 6-month post-transplantation. High-resolution (15-30 μM) micro-CT images were obtained in live mice under isoflurane anesthesia using Bruker's Skyscan 1278 micro-CT scanner. Anesthetized mice were positioned on a movable bed. To further minimize movement during scanning, the hindlimbs of the mice were taped to the bed. Only the hindlimbs were imaged, minimizing radiation dosage. Importantly, it has been established that radiation doses to mice are usually well below lethal doses (Boone et al., 2004). After the acquisition, 2D axial and 3D images were reconstructed for qualitative and quantitative analyses. For a region of interest measurement and analysis, axial images were displayed using the two- and three-dimensional biomedical image analysis software package (CT Bone Visualization and Analysis, Siemens Medical Solution Medical Solutions). Axial reformats were performed to allow slice-by-slice, manual tracing of the cortical and trabecular bone contours. For trabecular bone, a region of 183 $μm^2$ was analyzed approximately 250 μm below the growth plate, while cortical bone width was measured in a 183 $μm^2$ area in diaphysis around 4500 μm from the growth plate.

High-resolution *ex vivo* micro-CT was conducted six months post-transplantation. The individual tibia was fixed in 4% paraformaldehyde and stored in 70% ethanol until scanning. According to the rodent bone guidelines, the tibia was scanned in 70% ethanol using a cone-beam micro-CT system, μCT40 (Scanco Medical AG) (X-ray tube potential = 55 kVp, 8 μm isotropic nominal voxel size). Scans were exported to Analyze 12.0 software (AnalyzeDirect) for further analysis. The cortical region of interest was contoured on the exterior perimeter of each slice. At the same time, trabecular scans were contoured about the inner cortical circumference in an area located 180μm distal to the growth plate. The segmentation values for cortical bone were set at 0.8/½60, and analysis was done with a total of 102 consecutive 12- μm-thick sections, which were established semi-automatically. The segmentation values for trabecular bone were set at 0.8/½20, and analysis was done with a total of 208 consecutive six- μm-thick sections semi-automatically established.

All parameters are expressed in units following a standardized system of histomorphometric indices established by the ASBMR Histomorphometry Nomenclature Committee (Parfitt et al., 1987).

Mechanical testing

Femurs were mechanically tested using 3-point bending six months post-transplantation. An electro force system (ELF3200, EnduraTec) with a custom testing apparatus was used to test bones to failure at a constant displacement rate of 0.025 mm/s. Bones were tested in the posterior to the anterior direction so that the anterior side was in tension. A 50-lb load cell (Sensotec) measured the load applied, while mid-diaphyseal displacement was measured with a linear variable differential transducer. Load and displacement data were acquired using the WinTest system (EnduraTec). The resulting load-displacement curves were used to determine stiffness, maximum load, displacement, and post-yield displacement for each bone. Stiffness was measured as the slope of the linear region of the load-displacement curve in deflection. The maximum load was defined as the load attained before failure, with maximum displacement as the corresponding displacement. Post yield displacement was calculated as displacement at failure minus displacement at the yield point.

Bone histomorphometry

Tibiae from the PBS, WT, and OI Treg transplanted mice were embedded in methyl methacrylate (MMA), and slides were generated by the Research Histology Core at MD Anderson Cancer Center, according to the established Core protocols. The histomorphometric analyses were done by the Bone Histomorphometry Core of MD Anderson Cancer Center. Slides were stained with either Toluidine Blue or TRAP enzymatic stain with established Core protocols. Histomorphometric analysis of static parameters were performed using the Bioquant OSTEO II software platform. Tissue volume was analyzed by measuring 1.3mm from the

growth plate into the bone compartment, keeping 150μm away from the growth plate and cortical walls. The bone surface was analyzed by tracing the trabecular bone within the measurement area. Osteoclasts were counted if they were in contact with the trabecular bone surface and could be differentiated by their multi-nucleated structure. Osteoblasts were counted if they were in contact with the trabecular bone surface and had the classic cuboidal shape. Lining cells were excluded from the count. Osteoid was included in the analytical values where mineral deposits were identified along the bone surfaces. All parameters are expressed in units following a standardized system of histomorphometric indices established by the ASBMR Histomorphometry Nomenclature Committee (Parfitt et al., 1987)

Osteoblast cell culture

Long bones (tibia and femur) and calvaria, free of loose connective tissue, were cut into pieces, treated with crude collagenase P (Roche Diagnostic Corporation) and trypsin in PBS at 37°C for 10 min, and the supernatant discarded. Bone pieces were washed with α-MEM/10%FBS, and explant cultures were set up in α-MEM/10%FBS/1%penicillin/streptomycin (PS; 100 IU/mL penicillin G and 100 μg/mL streptomycin) for two weeks. Bone pieces were removed, and cells were grown for an additional week in α-MEM/10%FBS/1%PS/L-glutamine (L-glut; 2 mM, Sigma)/ascorbic acid 2-phosphate (AA; 200 μM, Wako Pure Chemical Industry) and replated for staining in the above-mentioned osteogenic media with β-glycerophosphate (BGP; 10 μM, Sigma) for three weeks.

Alizarin red staining

Alizarin Red staining kit (EMD Millipore Corporation) was used to detect deposited calcium salts per the manufacturer's instructions. Images were taken using Nikon Eclipse TS-100 inverted microscope. To quantify alizarin red staining, 10% cetylpyridinium chloride (CPC) in 10mM sodium phosphate was used to extract the alizarin red stain. The concentration was determined by reading the absorbance at 570 nm using an alizarin red standard curve. Each reading was done in triplicates.

Osteoclast cell culture

Bone marrow cells were flushed out of the femur and tibia with PBS, filtered to obtain a single-cell suspension, and centrifuged. Cells were cultured in α-MEM/10%FBS/10 ng/mL M-CSF/1%PS for 24 h at 37°C/5% CO_2 in a 100 mm dish. The supernatant was collected after 24 h and centrifuged to collect the non-adherent cells, which were plated in 24 well dishes at 10×10^6 cells per well and cultured for two days in the above media supplemented with 10 ng/mL murine recombinant M-CSF and 50 ng/mL RANKL. On day 3, media was replaced with the above media supplemented with 20 ng/mL M-CSF and 100 ng/mL RANKL. On day 5, media was changed with the day 3 media to induce mature osteoclasts for 7-8 days.

TARTRATE-RESISTANT ACID PHOSPHATASE (TRAP) STAINING

According to the manufacturer's instructions, TRAP staining was performed in the cells using the leukocyte acid phosphatase kit (Sigma Aldrich). Images of various areas of the well were taken using a Nikon Eclipse TS-100 inverted microscope. Three wells per group were used to count the osteoclasts. TRAP⁺ cells containing three or more nuclei were counted as osteoclasts.

BONE RESORPTION ASSAY

A bone resorption assay kit was purchased from CosmoBio and was used to evaluate the osteoclast bone resorption activity according to the manufacturer's protocol. Briefly, bone marrow cells (2×10^6 cells/well) were cultured in the coated plate (supplied with the kit), supplemented with 20 ng/mL M-CSF and 100 ng/mL RANKL. The media was changed with every day 3 until the formation of mature osteoclasts was observed. For fixing, media was removed, and 5% sodium hypochlorite was added for 3-5 min. After washing the plate with water and drying, photographs of 9–10 regions in each well were taken (taking care not that the areas do not overlap). The transparent areas on the images were counted as pits manually.

Microscopy

Wells were imaged using the Nikon Eclipse TS-100 inverted microscope and EVOS M5000 Imaging System. The brightness and contrast of the images were adjusted using Adobe Photoshop CS2 software. The same parameters were applied to an individual group of images.

QUANTIFICATION AND STATISTICAL ANALYSIS

All statistical analyses were performed using the GraphPad Prism 6.0 software (GraphPad Software, Inc.). Each experiment included 7-9 mice per group. Age-matched recipient and donor mice of both genders were included and randomly assigned to groups. The percentage of males and females used as transplant recipients was 56% and 44%, respectively. Data are presented as Mean ± SD. Unpaired two-tailed Student's t test and one-way ANOVA were used to calculate p values for two-group and multigroup datasets. For the longitudinal micro-CT analysis, Repeated Measures ANOVA was used to calculate the statistical significance. A value of $p \leq 0.05$ was regarded as statistically significant. The statistical values and details of the experiments can be found in the respective figures, figure legends and results.